

# GSP-Based MAP Estimation of Graph Signals

Guy Sagi and Tirza Routtenberg, *Senior Member, IEEE*

**Abstract**—In this paper, we consider the problem of recovering random graph signals from nonlinear measurements. We formulate the maximum *a-posteriori* probability (MAP) estimator, which results in a nonconvex optimization problem. Conventional iterative methods for minimizing nonconvex problems are sensitive to the initialization, have high computational complexity, and do not utilize the underlying graph structure behind the data. In this paper we propose two new estimators that are both based on the Gauss-Newton method: 1) the elementwise graph-frequency-domain MAP (eGFD-MAP) estimator; and 2) the graph signal processing MAP (GSP-MAP) estimator. At each iteration, these estimators are updated by the outputs of two graph filters, with the previous state estimator and the residual as the input graph signals. The eGFD-MAP estimator is an ad-hoc method that minimizes the MAP objective function in the graph frequency domain and neglects mixed-derivatives of different graph frequencies in the Jacobian matrix as well as off-diagonal elements in the covariance matrices. Consequently, it updates the elements of the graph signal independently, which reduces the computational complexity compared to the conventional MAP estimator. The GSP-MAP estimator is based on optimizing the graph filters at each iteration of the Gauss-Newton algorithm. We state conditions under which the eGFD-MAP and GSP-MAP estimators coincide with the MAP estimator, in the case of an observation model with orthogonal graph frequencies. We evaluate the performance of the estimators for nonlinear graph signal recovery tasks with synthetic data and with the real-world problem of state estimation in power systems. These simulations show the advantages of the proposed estimators in terms of computational complexity, mean-squared-error, and robustness to the initialization of the iterative algorithms.

**Index Terms**—Graph signal processing (GSP), graph filters, graph-frequency domain, nonlinear estimation, maximum *a-posteriori* probability (MAP) estimation

## I. INTRODUCTION

The emerging field of graph signal processing (GSP) deals with processing data indexed by general graphs with concepts and techniques inspired by traditional digital signal processing (DSP). These techniques include graph Fourier transforms (GFT), graph filter designs [1]–[4], and the sampling and recovery of graph signals [5]–[7]. Most of these techniques have been used for various tasks under a linear measurement model. However, modern networks are often large and complex, contain heterogeneous large datasets, and are characterized by nonlinear models [8], [9], and as a result, graph signals are often difficult to recover in these networks. Examples of applications with such networks include brain network

connectivity [10], environmental monitoring [11], and power flow equations in power systems [12]–[14]. Hence, the development of GSP methods for the estimation of graph signals in nonlinear models has considerable practical significance.

The mean-squared-error (MSE) is one of the most commonly-used criteria of accuracy for estimation and reconstruction purposes. In Bayesian estimation, the optimal minimum MSE (MMSE) estimator usually lacks a closed-form expression in nonlinear models and is often computationally intractable. Therefore, the linear MMSE (LMMSE) estimator and other low-complexity estimators (e.g. [15]–[17]) are widely used in practice. The linear GSP-LMMSE estimator, which minimizes the MSE among estimators that are represented as an output of a graph filter, has been suggested in [18] for the recovery of graph signals, and its properties are discussed. In particular, it has been shown that the GSP-LMMSE estimator has low computational complexity, and the ability to adapt to changes in the graph topology. In addition, it has been extended to a widely-linear estimation of complex-valued signals in [19]. However, linear estimators fail to take into account the nonlinearity of the measurement model, which may lead to degraded performance compared with nonlinear methods. Consequently, developing nonlinear estimation methods that take advantage of the graph structure and GSP theory have the potential to significantly improve the estimation performance.

Nonlinear methods can significantly outperform linear estimators in terms of MSE. For example, the superiority of the nonlinear maximum *a-posteriori* probability (MAP) estimator compared with the LMMSE estimator in nonlinear filtering is well known [20]. In order to implement nonlinear methods, such as the MAP estimator, in nonlinear settings, iterative methods are used such as the widely-employed Gauss-Newton method. However, the Gauss-Newton method is sensitive to initialization, and may converge to a local minima or even diverge [21], [22]. Thus, integrating the graph information, e.g. by using graph filters, has the potential to enhance the robustness of iterative implementations of the MAP estimator.

Graph filters have been used for many signal processing tasks, such as denoising [23], [24], classification [25], and anomaly detection [12]. Model-based recovery of graph signals by GSP filters for linear models was treated in [3], [23], [26], [27]. Nonlinear graph filters were considered in [11], but they require higher-order statistics that are not completely specified in the general nonlinear case. Recently, graph neural network approaches were considered in [28], [29]. In addition, a Gauss-Newton unrolled neural network method was developed in [30] for the application of power system state estimation (PSSE). However, data-based methods necessitate extensive stationary training sets, and do not necessarily utilize the model information. Using the model at hand, one can design estimators with improved performance in terms of

G. Sagi and T. Routtenberg are with the School of Electrical and Computer Engineering, Ben-Gurion University of the Negev, Beer Sheva, Israel. Tirza Routtenberg is also with the Department of Electrical and Computer Engineering, Princeton University, Princeton, NJ 08544 USA. This work has been submitted to the IEEE for possible publication. Copyright may be transferred without notice, after which this version may no longer be accessible.

e-mail: sagix@post.bgu.ac.il, tirzar@bgu.ac.il. This work is partially supported by the Israeli Ministry of National Infrastructure, Energy, and Water Resources.

MSE, interpretability, robustness, complexity, and flexibility. Fitting graph-based models to given data was considered in [31]–[33]. However, model-fitting approaches aim to minimize the modeling error, and in general have significantly lower performance than estimators that minimize the estimation error directly [34].

In this paper, we consider the nonlinear estimation of random graph signals with a nonlinear observation model and a Gaussian distribution. First, we present the MAP estimator, as well as its implementations in the vertex and in the graph-frequency domains by using the Gauss-Newton method. Then, we propose two new GSP estimators: 1) the elementwise graph-frequency-domain MAP (eGFD-MAP) estimator; and 2) the GSP-MAP estimator. The eGFD-MAP estimator updates the coordinates of the estimator in the graph-frequency domain separately, and has a significantly lower computational complexity than the MAP estimator. The GSP-MAP estimator is based on optimizing the graph filters at each iteration of the Gauss-Newton algorithm. We discuss the conditions under which the eGFD-MAP and the GSP-MAP estimators coincide with the MAP estimator. In particular, we show that for models with measurement functions that have orthogonal graph frequencies, i.e. separable in the graph-frequency domain, the eGFD-MAP and the GSP-MAP estimators coincide with the MAP estimator. We perform numerical simulations for: 1) synthetic data with orthogonal graph frequencies; and 2) power system state estimation (PSSE). For the first case, it is shown that the eGFD-MAP and the GSP-MAP estimators achieve the same MSE as the MAP estimator, while the eGFD-MAP estimator significantly reduces the computational complexity, especially in large networks where the MAP and the GSP-MAP estimators are intractable. For the PSSE simulations, it is shown that the eGFD-MAP and the GSP-MAP estimators almost achieve the performance of the MAP estimator, and significantly outperform the linear estimator. Moreover, the proposed eGFD-MAP and GSP-MAP estimators are more robust to perturbed initialization than the MAP estimator.

The rest of this paper is organized as follows. In Section II we introduce the basics of GSP required for this paper. In Section III, we formulate the estimation problem, present the MAP estimation approaches (in the vertex and graph-frequency domains), and describe the Gauss-Newton implementation of the MAP estimators. In Section IV, we develop the eGFD-MAP and GSP-MAP estimators and discuss their properties. Simulations are presented in Section V. Finally, conclusions are outlined in Section VI.

In the following, we denote vectors by boldface lowercase letters and matrices by boldface uppercase letters. The operators  $(\cdot)^T$  and  $(\cdot)^{-1}$  denote the transpose and inverse, respectively. The vector  $\mathbf{1}$  denotes a vector of all ones, and  $\circ$  denotes the Hadamard product. The  $m$ th element of the vector  $\mathbf{a}$  is denoted by  $a_m$  or  $[\mathbf{a}]_m$ . The  $(m, q)$ th element of the matrix  $\mathbf{A}$  is written as  $A_{m,q}$  or  $[\mathbf{A}]_{m,q}$ . For a vector  $\mathbf{a}$ ,  $\text{diag}(\mathbf{a})$  is a diagonal matrix whose  $i$ th diagonal entry is  $a_i$ ; when applied to a matrix,  $\text{diag}(\mathbf{A})$  is a vector collecting the diagonal elements of  $\mathbf{A}$ . In addition,  $\text{ddiag}(\mathbf{A}) = \text{diag}(\text{diag}(\mathbf{A}))$  is the diagonal matrix whose entries on the diagonal are those of  $\mathbf{A}$ . The identity matrix and the zero vector are written as  $\mathbf{I}$  and  $\mathbf{0}$ , respectively. The cross-covariance matrix of the vectors

$\mathbf{a}$  and  $\mathbf{b}$  is denoted by  $\mathbf{C}_{\mathbf{ab}} \triangleq \mathbb{E}[(\mathbf{a} - \mathbb{E}[\mathbf{a}])(\mathbf{b} - \mathbb{E}[\mathbf{b}])^T]$ . The Jacobian matrix of a vector function  $\mathbf{g}(\mathbf{x})$ ,  $\nabla_{\mathbf{x}}\mathbf{g}(\mathbf{x})$ , is a matrix in  $\mathbb{R}^{K \times M}$ , with the  $(k, m)$ th element equal to  $\frac{\partial g_k}{\partial x_m}$ , where  $\mathbf{g} = [g_1, \dots, g_K]^T$  and  $\mathbf{x} = [x_1, \dots, x_M]^T$ . We use the notation  $\nabla_{\mathbf{x}}^T \mathbf{g}(\mathbf{x}) \triangleq (\nabla_{\mathbf{x}} \mathbf{g}(\mathbf{x}))^T$ . For a scalar function,  $g(\mathbf{x})$ , we denote  $\nabla_{\mathbf{x}}^2 g(\mathbf{x}) \triangleq \nabla_{\mathbf{x}} \nabla_{\mathbf{x}}^T g(\mathbf{x})$ . Finally,  $\|\cdot\|$  denotes the Euclidean norm.

## II. BACKGROUND: GRAPH SIGNAL PROCESSING (GSP)

Consider an undirected, connected, weighted graph  $\mathcal{G}(\mathcal{V}, \xi, \mathbf{W})$ , where  $\mathcal{V}$  and  $\xi$  are sets of vertices and edges, respectively. The matrix  $\mathbf{W} \in \mathbb{R}^{N \times N}$  is the nonnegative weighted adjacency matrix of the graph, where  $N \triangleq |\mathcal{V}|$  is the number of vertices in the graph. If there is an edge  $(i, j) \in \xi$  connecting vertices  $i$  and  $j$ , the entry  $\mathbf{W}_{i,j}$  represents the weight of the edge; otherwise,  $\mathbf{W}_{i,j} = 0$ . The Laplacian matrix of this graph is defined by  $\mathbf{L} \triangleq \text{diag}(\mathbf{W}\mathbf{1}) - \mathbf{W}$ . The Laplacian matrix,  $\mathbf{L}$ , is a real and positive semidefinite matrix; thus, its associated eigenvalue decomposition is given by

$$\mathbf{L} = \mathbf{V}\mathbf{\Lambda}\mathbf{V}^T, \quad (1)$$

where  $\mathbf{\Lambda}$  is a diagonal matrix consisting of the eigenvalues of  $\mathbf{L}$ ,  $0 = \lambda_1 < \lambda_2 \leq \dots \leq \lambda_N$ ,  $\mathbf{V}$  is a matrix whose  $n$ th column,  $\mathbf{v}_n$ , is the eigenvector of  $\mathbf{L}$  that is associated with  $\lambda_n$ , and  $\mathbf{V}^T = \mathbf{V}^{-1}$ .

In this paper, a *graph signal* is an  $N$ -dimensional vector,  $\mathbf{a}$ , that assigns a scalar value to each vertex, i.e. each entry  $a_n$  denotes the signal value at vertex  $n$ , for  $n = 1, \dots, N$ . The GFT of the graph signal  $\mathbf{a}$  is defined as [2]

$$\tilde{\mathbf{a}} \triangleq \mathbf{V}^T \mathbf{a}. \quad (2)$$

Similarly, the inverse GFT (IGFT) of  $\tilde{\mathbf{a}}$  is given by  $\mathbf{V}\tilde{\mathbf{a}}$ . A graph signal is a graph-bandlimited signal with cutoff graph frequency  $N_s$  if it satisfies [1]

$$\tilde{a}_n = 0, \quad n = N_s + 1, \dots, N. \quad (3)$$

Graph filters are useful tools for various GSP tasks. Linear and shift-invariant graph filters with respect to (w.r.t.) the graph shift operator (GSO) play essential roles in GSP. A graph filter is a function  $f(\cdot)$  applied to a GSO, where here we use the Laplacian  $\mathbf{L}$  as the GSO, which allows the following eigendecomposition [1]:

$$f(\mathbf{L}) = \mathbf{V}f(\mathbf{\Lambda})\mathbf{V}^T, \quad (4)$$

where  $f(\mathbf{\Lambda})$  is a diagonal matrix. That is,  $f(\lambda_n)$  is the graph frequency response of the filter at graph frequency  $\lambda_n$ ,  $n = 1, \dots, N$ , and  $f(\mathbf{L})$  is diagonalized by the eigenvector matrix of  $\mathbf{L}$ ,  $\mathbf{V}$ . We assume that the graph filter,  $f(\cdot)$ , is a well-defined function on the spectrum of  $\mathbf{L}$ ,  $\{\lambda_1, \dots, \lambda_N\}$ .

## III. MAP ESTIMATOR OF GRAPH SIGNALS

In this section we formulate the MAP estimator for the problem of estimating a random graph signal by observing its noisy nonlinear function. First, the measurement model and assumption are introduced in Subsection III-A. Then, we derive the MAP estimator in both the vertex and the graph-frequency domains in Subsection III-B. In Subsection III-C, we show the implementation of the MAP estimator by the Gauss-Newton method.

### A. Model

Consider the problem of recovering a random input graph signal,  $\mathbf{x} \in \mathbb{R}^N$ , based on the following nonlinear measurement model:

$$\mathbf{y} = \mathbf{g}(\mathbf{L}, \mathbf{x}) + \mathbf{w}, \quad (5)$$

where the measurement function,  $\mathbf{g} : \mathbb{R}^{N \times N} \times \mathbb{R}^N \rightarrow \mathbb{R}^N$ , and the Laplacian matrix,  $\mathbf{L}$ , which represents the influence of the graph topology, are assumed to be known. In addition, it is assumed that  $\mathbf{g}(\mathbf{L}, \mathbf{x})$  is continuously differentiable w.r.t.  $\mathbf{x}$ . We assume that the graph input signal,  $\mathbf{x}$ , is a Gaussian vector with mean  $\boldsymbol{\mu}_x$  and covariance matrix  $\mathbf{C}_{xx}$ . The noise,  $\mathbf{w}$ , is assumed to be a zero-mean Gaussian vector with covariance matrix  $\mathbf{C}_{ww}$ . Finally, we assume that  $\mathbf{w}$  and  $\mathbf{x}$  are independent. The nonlinear measurement model in (5) is adequate for many applications within networked data and the Internet-of Things (IoT) [18], [35], [36]. In particular, this model arises in PSSE, which is discussed in Section V.

### B. MAP estimator

In the following, we develop the MAP estimator for the measurement model in (5). The MAP estimator of  $\mathbf{x}$  from  $\mathbf{y}$  is given by

$$\hat{\mathbf{x}} = \underset{\mathbf{x} \in \mathbb{R}^N}{\operatorname{argmax}} f(\mathbf{x}|\mathbf{y}) = \underset{\mathbf{x} \in \mathbb{R}^N}{\operatorname{argmax}} \log f(\mathbf{y}|\mathbf{x}) + \log f(\mathbf{x}), \quad (6)$$

where the second equality is obtained by using Bayes's rule, applying the monotonically-increasing logarithm function and removing constant terms w.r.t.  $\mathbf{x}$ . By substituting the considered model, in which  $\mathbf{y}$  given  $\mathbf{x}$  is also a Gaussian vector with mean  $\mathbf{g}(\mathbf{L}, \mathbf{x})$  and covariance  $\mathbf{C}_{ww}$ , in (6), we obtain

$$\hat{\mathbf{x}} = \underset{\mathbf{x} \in \mathbb{R}^N}{\operatorname{argmin}} Q(\mathbf{x}), \quad (7)$$

where, after removing constant terms w.r.t.  $\mathbf{x}$ , we have

$$Q(\mathbf{x}) \triangleq \frac{1}{2}(\mathbf{x} - \boldsymbol{\mu}_x)^T \mathbf{C}_{xx}^{-1}(\mathbf{x} - \boldsymbol{\mu}_x) + \frac{1}{2}(\mathbf{y} - \mathbf{g}(\mathbf{L}, \mathbf{x}))^T \mathbf{C}_{ww}^{-1}(\mathbf{y} - \mathbf{g}(\mathbf{L}, \mathbf{x})). \quad (8)$$

The left term in the objective function on the r.h.s. of (8) corresponds to the prior, and the right term corresponds to the noisy measurement model. This objective function can be minimized by iterative algorithms to approximate the MAP estimator, as described in Section III-C. The objective function in (8) discards information about the relationship between the graph signal and its underlying graph structure. As a result, it is less robust to perturbations of the initialization that are due to changes in the graph topology. In addition, the MAP estimator only uses the measurement function and does not exploit additional GSP information on the graph signal, such as smoothness or graph-bandlimitness, that can be utilized to improve estimation performance.

In general, representing data in the graph-frequency domain can yield substantial data reduction, and minimize the computational requirements and memory use. Thus, as a first step, we suggest to transform  $Q(\mathbf{x})$  into its graph-frequency domain representation (as a function of  $\tilde{\mathbf{x}}$ ):

$$Q_{freq}(\tilde{\mathbf{x}}) \triangleq \frac{1}{2}(\tilde{\mathbf{x}} - \tilde{\boldsymbol{\mu}}_x)^T \mathbf{C}_{\tilde{x}\tilde{x}}^{-1}(\tilde{\mathbf{x}} - \tilde{\boldsymbol{\mu}}_x) + \frac{1}{2}(\tilde{\mathbf{y}} - \tilde{\mathbf{g}}(\mathbf{L}, \mathbf{V}\tilde{\mathbf{x}}))^T \mathbf{C}_{\tilde{w}\tilde{w}}^{-1}(\tilde{\mathbf{y}} - \tilde{\mathbf{g}}(\mathbf{L}, \mathbf{V}\tilde{\mathbf{x}})), \quad (9)$$

where  $\tilde{\mathbf{y}}$ ,  $\tilde{\mathbf{x}}$ ,  $\tilde{\boldsymbol{\mu}}_x$ , and  $\tilde{\mathbf{g}}$  are the GFT representations of  $\mathbf{y}$ ,  $\mathbf{x}$ ,  $\boldsymbol{\mu}_x$ , and  $\mathbf{g}$ , respectively, as defined in (2), such that  $\tilde{\mathbf{g}}(\mathbf{L}, \mathbf{V}\tilde{\mathbf{x}}) = \mathbf{V}^T \mathbf{g}(\mathbf{L}, \mathbf{x})$ . In addition, we use the fact that

$$\mathbf{C}_{\tilde{x}\tilde{x}} \triangleq \mathbb{E}[\mathbf{V}^T(\mathbf{x} - \boldsymbol{\mu}_x)(\mathbf{x} - \boldsymbol{\mu}_x)^T \mathbf{V}] = \mathbf{V}^T \mathbf{C}_{xx} \mathbf{V}$$

and similarly  $\mathbf{C}_{\tilde{w}\tilde{w}} = \mathbf{V}^T \mathbf{C}_{ww} \mathbf{V}$ . It can be verified that the r.h.s. of (8) and the r.h.s. of (9) are identical. Thus, these two objective functions will lead to the same final estimator, where in (8) the update is in the vertex domain ( $\mathbf{x}$ ), and in (9) the update is in the graph-frequency domain ( $\tilde{\mathbf{x}}$ ). It should be noted that the efficiency and the convergence rate of the specific implementation in each domain may be different. For example, in our simulations (see Subsection V), we realized that implementing the MAP estimator in the graph-frequency domain is much faster.

### C. Implementation by Gauss-Newton method

Since  $\mathbf{g}(\mathbf{L}, \mathbf{x})$  is a nonlinear and nonconvex function, direct minimization of the objective functions in (8), (9), or (17) is intractable. Numerous algorithms have been proposed to minimize nonconvex objectives. Here, we implement the Gauss-Newton method, which is widely employed to solve nonlinear weighted least squares (WLS) problems and to find the MAP estimator. The Gauss-Newton method has the desirable property of a quadratic rate of convergence under suitable assumptions [22].

**Initialization:** For all the algorithms described in this and in the following section, the estimators can be initialized by the prior mean, i.e.  $\hat{\mathbf{x}}^{(0)} = \boldsymbol{\mu}_x$  and  $\hat{\tilde{\mathbf{x}}}^{(0)} = \tilde{\boldsymbol{\mu}}_x$ , where  $\tilde{\boldsymbol{\mu}}_x \triangleq \mathbf{V}^T \boldsymbol{\mu}_x$ . Alternatively, if training data is available or can be generated, it is possible to initialize the estimators by the LMMSE or the GSP-LMMSE [18] estimators. In addition, the stopping condition is attained when two successive MAP estimates,  $\hat{\mathbf{x}}^{(t+1)}$  and  $\hat{\mathbf{x}}^{(t)}$ , are sufficiently close, where  $t$  is the iteration index.

1) *Conventional MAP estimator:* In order to locally minimize the MAP cost function in (8), we use the Gauss-Newton method, which relies on Taylor's expansion to linearize the measurement function  $\mathbf{g}(\mathbf{L}, \mathbf{x})$  and iteratively updates the estimators until convergence (see Sec. 1.5.1 in [37]). Specifically, under the assumption that the given estimator  $\hat{\mathbf{x}}^{(t)}$  is close enough to  $\mathbf{x}$ , the linear first-order approximation of  $\mathbf{g}(\mathbf{L}, \mathbf{x})$  is

$$\mathbf{g}(\mathbf{L}, \mathbf{x}) \approx \mathbf{g}(\mathbf{L}, \hat{\mathbf{x}}^{(t)}) + \mathbf{G}(\mathbf{L}, \hat{\mathbf{x}}^{(t)})(\mathbf{x} - \hat{\mathbf{x}}^{(t)}), \quad (10)$$

where

$$\mathbf{G}(\mathbf{L}, \hat{\mathbf{x}}^{(t)}) \triangleq \nabla_{\mathbf{x}} \mathbf{g}(\mathbf{L}, \mathbf{x})|_{\mathbf{x}=\hat{\mathbf{x}}^{(t)}} \quad (11)$$

is the  $N \times N$  Jacobian matrix of the measurement function  $\mathbf{g}(\mathbf{L}, \mathbf{x})$  evaluated at  $\hat{\mathbf{x}}^{(t)}$ . By substituting the approximation from (10) in (8), we obtain the approximated linearized objective function:

$$Q(\mathbf{x}) \approx Q_{lin}(\mathbf{x}, \hat{\mathbf{x}}^{(t)}) \triangleq \frac{1}{2}(\mathbf{x} - \boldsymbol{\mu}_x)^T \mathbf{C}_{xx}^{-1}(\mathbf{x} - \boldsymbol{\mu}_x) + \frac{1}{2}(\mathbf{y} - \mathbf{g}(\mathbf{L}, \hat{\mathbf{x}}^{(t)}) - \mathbf{G}(\mathbf{L}, \hat{\mathbf{x}}^{(t)})(\mathbf{x} - \hat{\mathbf{x}}^{(t)}))^T \mathbf{C}_{ww}^{-1} \times (\mathbf{y} - \mathbf{g}(\mathbf{L}, \hat{\mathbf{x}}^{(t)}) - \mathbf{G}(\mathbf{L}, \hat{\mathbf{x}}^{(t)})(\mathbf{x} - \hat{\mathbf{x}}^{(t)})). \quad (12)$$

The Gauss-Newton method finds the next iterate  $t + 1$  by minimizing  $Q_{lin}(\mathbf{x}, \hat{\mathbf{x}}^{(t)})$  w.r.t.  $\mathbf{x}$ , which results in

$$\begin{aligned} \hat{\mathbf{x}}^{(t+1)} &= \arg \min_{\mathbf{x} \in \mathbb{R}^N} Q_{lin}(\mathbf{x}, \hat{\mathbf{x}}^{(t)}) \\ &= \hat{\mathbf{x}}^{(t)} - \alpha^{(t)} \left( \mathbf{C}_{\mathbf{xx}}^{-1} + \mathbf{G}^T(\mathbf{L}, \hat{\mathbf{x}}^{(t)}) \mathbf{C}_{\mathbf{ww}}^{-1} \mathbf{G}(\mathbf{L}, \hat{\mathbf{x}}^{(t)}) \right)^{-1} \\ &\quad \times \left( \mathbf{C}_{\mathbf{xx}}^{-1} (\hat{\mathbf{x}}^{(t)} - \boldsymbol{\mu}_{\mathbf{x}}) \right. \\ &\quad \left. - \mathbf{G}^T(\mathbf{L}, \hat{\mathbf{x}}^{(t)}) \mathbf{C}_{\mathbf{ww}}^{-1} (\mathbf{y} - \mathbf{g}(\mathbf{L}, \hat{\mathbf{x}}^{(t)})) \right), \end{aligned} \quad (13)$$

with  $\alpha^{(t)} = 1$ .

In practice, wisely setting the step size,  $\alpha^{(t)} \in (0, 1]$ , can improve the convergence rate [38]. In this paper, we compute the step size by a backtracking line search (Algorithm 2). In this strategy, we iteratively reduce the step size,  $\alpha^{(t)}$ , until  $\hat{\mathbf{x}}^{(t+1)}$  from (13) with the tested step size that satisfies

$$Q(\hat{\mathbf{x}}^{(t)}) - Q(\hat{\mathbf{x}}^{(t+1)}) > \Delta |Q(\hat{\mathbf{x}}^{(t)})|, \quad (14)$$

where  $\Delta \in \mathbb{R}$  satisfies  $\Delta \ll 1$ . The MAP-estimator algorithm is summarized in Algorithm 1.

---

#### Algorithm 1: MAP estimator by Gauss-Newton

---

**Input:**

- The function  $\mathbf{g}(\mathbf{L}, \mathbf{x})$
- The mean and covariance matrices  $\boldsymbol{\mu}_{\mathbf{x}}$ ,  $\mathbf{C}_{\mathbf{xx}}$ , and  $\mathbf{C}_{\mathbf{ww}}$
- Initial step size  $\alpha_0$ ,  $\gamma$  and  $\Delta$
- The tolerance  $\delta$

**Algorithm Steps:**

- 1) Initialization:  $\hat{\mathbf{x}}^{(0)}$
- 2) Compute:  $\mathbf{g}(\mathbf{L}, \hat{\mathbf{x}}^{(t)})$  and  $\mathbf{G}(\mathbf{L}, \hat{\mathbf{x}}^{(t)})$  from (11)
- 3) Choose step size  $\alpha^{(t)}$  such that (14) holds using Algorithm 2 with the cost  $Q$  from (8)
- 4) Compute  $\mathbf{x}^{(t+1)}$  from (13) with step size  $\alpha^{(t)}$
- 5) Stopping condition:  $\|\hat{\mathbf{x}}^{(t+1)} - \hat{\mathbf{x}}^{(t)}\| < \delta$

**Output:** MAP estimator  $\hat{\mathbf{x}} = \hat{\mathbf{x}}^{(t+1)}$

---

2) *MAP estimator in the graph-frequency domain:* In this subsection, we evaluate the graph-frequency-domain update of the MAP estimator. Similar to the derivation of (13), the minimization of  $Q_{freq}(\tilde{\mathbf{x}})$  from (9) w.r.t.  $\tilde{\mathbf{x}}$  by the Gauss-Newton method results in the following update equation:

$$\begin{aligned} \hat{\tilde{\mathbf{x}}}^{(t+1)} &= \hat{\tilde{\mathbf{x}}}^{(t)} \\ &\quad - \alpha^{(t)} \left( \mathbf{C}_{\tilde{\mathbf{x}\tilde{\mathbf{x}}}}^{-1} + \tilde{\mathbf{G}}^T(\mathbf{L}, \mathbf{V}\hat{\tilde{\mathbf{x}}}^{(t)}) \mathbf{C}_{\tilde{\mathbf{w}\tilde{\mathbf{w}}}}^{-1} \tilde{\mathbf{G}}(\mathbf{L}, \mathbf{V}\hat{\tilde{\mathbf{x}}}^{(t)}) \right)^{-1} \\ &\quad \times \left( \mathbf{C}_{\tilde{\mathbf{x}\tilde{\mathbf{x}}}}^{-1} (\hat{\tilde{\mathbf{x}}}^{(t)} - \tilde{\boldsymbol{\mu}}_{\tilde{\mathbf{x}}}) \right. \\ &\quad \left. - \tilde{\mathbf{G}}^T(\mathbf{L}, \mathbf{V}\hat{\tilde{\mathbf{x}}}^{(t)}) \mathbf{C}_{\tilde{\mathbf{w}\tilde{\mathbf{w}}}}^{-1} (\tilde{\mathbf{y}} - \tilde{\mathbf{g}}(\mathbf{L}, \mathbf{V}\hat{\tilde{\mathbf{x}}}^{(t)})) \right), \end{aligned} \quad (15)$$

where

$$\tilde{\mathbf{G}}(\mathbf{L}, \mathbf{V}\tilde{\mathbf{x}}) \triangleq \nabla_{\tilde{\mathbf{x}}} \tilde{\mathbf{g}}(\mathbf{L}, \mathbf{V}\tilde{\mathbf{x}}) = \mathbf{V}^T \mathbf{G}(\mathbf{L}, \mathbf{x}) \mathbf{V}. \quad (16)$$

It can be verified that by multiplying (13) by  $\mathbf{V}^T$  from the left, we obtain the iteration in the graph-frequency domain in (15). In addition, it is known that the convergence of the Gauss-Newton method is invariant under affine transformations of the domain [39]. An advantage of the update in (15) compared with (13) is for cases where  $\mathbf{x}$  is a graph bandlimited

---

#### Algorithm 2: Backtracking line search

---

**Input:**

- Current estimator  $\hat{\mathbf{x}}^{(t)}$
- Initial step size  $\alpha_0 \in (0, 1]$ , tuning parameter  $\gamma \in (0, 1)$
- Cost function  $Q$

**Algorithm Steps:**

- 1) Compute:  $Q(\hat{\mathbf{x}}^{(t)})$
- 2) **for**  $k = 0, 1, \dots, K_{\max}$  **do**
  - Compute  $\hat{\mathbf{x}}^{(t+1)}$  with  $\alpha^{(t)} = \alpha_k$
  - Compute  $Q(\hat{\mathbf{x}}^{(t+1)})$
- if** (14) *does not hold* **then**
  - if**  $k = K_{\max}$  **then**
    - |  $\alpha_{K_{\max}} = 0$
  - end**
  - else**
    - |  $\alpha_{k+1} = \gamma \alpha_k$
  - end**
- end**
- else**
  - | **break**
- end**
- end**

**Output:** Step size:  $\alpha^{(t)} = \alpha_k$

---

signal with a cutoff graph frequency  $N_s$ . In this case, we substitute  $[\hat{\tilde{\mathbf{x}}}^{(t)}]_n = 0 \forall n > N_s$  and update only the first  $N_s$  elements of  $\hat{\tilde{\mathbf{x}}}^{(t+1)}$  in (15) at each step. The MAP estimator in the graph frequency domain can be implemented using Algorithm 1, with the cost  $Q$  from (9) in step 3) and with (15) instead of (13) in step 4) of the algorithm. In terms of computational complexity, implementing the MAP estimator by (13) and (15) requires the computation of the inverse of  $N \times N$  matrices  $\mathbf{C}_{\mathbf{xx}}^{-1} + \mathbf{G}^T(\mathbf{L}, \hat{\mathbf{x}}^{(t)}) \mathbf{C}_{\mathbf{ww}}^{-1} \mathbf{G}(\mathbf{L}, \hat{\mathbf{x}}^{(t)})$  in (13), or  $\mathbf{C}_{\tilde{\mathbf{x}\tilde{\mathbf{x}}}}^{-1} + \tilde{\mathbf{G}}^T(\mathbf{L}, \mathbf{V}\hat{\tilde{\mathbf{x}}}^{(t)}) \mathbf{C}_{\tilde{\mathbf{w}\tilde{\mathbf{w}}}}^{-1} \tilde{\mathbf{G}}(\mathbf{L}, \mathbf{V}\hat{\tilde{\mathbf{x}}}^{(t)})$  in (15) in addition to multiplications of  $N \times N$  matrices at each iteration, which leads to high computational complexity. Furthermore, due to the nonconvexity of  $\mathbf{g}(\mathbf{L}, \mathbf{x})$  and the quadratic loss function, the Gauss-Newton method is sensitive to initialization and may diverge. These challenges inhibit its use for real-time estimation in large-scale networks. Moreover, these methods do not utilize the information about the underlying graph structure, e.g. for the initialization approach. Thus, they are less robust to changes and misspecification in the graph topology, e.g. in the graph connectivity. Finally, the estimators in (13) and (15) ignore the GSP properties and do not exploit additional information on the graph signal, such as smoothness or graph-bandlimitness, that can improve estimation performance.

## IV. EGFD-MAP AND GSP-MAP ESTIMATORS

In this section, we propose two new estimators that integrate the graph structure: the eGFD-MAP in Subsection IV-A and the GSP-MAP in Subsection IV-B. In Subsection IV-C, we present special cases and discuss the conditions under which the proposed eGFD-MAP and GSP-MAP estimators coincide with the MAP estimator. Finally, in Subsection IV-D we compare the computational complexity of the different estimators.

### A. eGFD-MAP estimator

In the nonlinear case, numerical optimization methods are usually used to minimize (8) or (9). However, when  $N$  is large, the minimization problem is high-dimensional, with high computational complexity and memory demands. In order to reduce the complexity and accelerate the convergence rate of the iterative optimization algorithms, we propose here the eGFD-MAP estimator, which is based on two steps. In the first step, we replace the MAP objective function from (9) by the following objective function in the graph-frequency domain:

$$\begin{aligned} Q_{freq}^{(d)}(\tilde{\mathbf{x}}) &\triangleq \frac{1}{2}(\tilde{\mathbf{x}} - \tilde{\boldsymbol{\mu}}_{\mathbf{x}})^T \mathbf{D}_{\tilde{\mathbf{x}}\tilde{\mathbf{x}}}^{(inv)}(\tilde{\mathbf{x}} - \tilde{\boldsymbol{\mu}}_{\mathbf{x}}) \\ &\quad + \frac{1}{2}(\tilde{\mathbf{y}} - \tilde{\mathbf{g}}(\mathbf{L}, \mathbf{V}\tilde{\mathbf{x}}))^T \mathbf{D}_{\tilde{\mathbf{w}}\tilde{\mathbf{w}}}^{(inv)}(\tilde{\mathbf{y}} - \tilde{\mathbf{g}}(\mathbf{L}, \mathbf{V}\tilde{\mathbf{x}})) \\ &= \frac{1}{2} \sum_{n=1}^N (\tilde{x}_n - [\tilde{\boldsymbol{\mu}}_{\mathbf{x}}]_n)^2 [\mathbf{C}_{\tilde{\mathbf{x}}\tilde{\mathbf{x}}}^{-1}]_{n,n} \\ &\quad + \frac{1}{2} \sum_{n=1}^N (\tilde{y}_n - [\tilde{\mathbf{g}}(\mathbf{L}, \mathbf{V}\tilde{\mathbf{x}})]_n)^2 [\mathbf{C}_{\tilde{\mathbf{w}}\tilde{\mathbf{w}}}^{-1}]_{n,n}, \end{aligned} \quad (17)$$

where

$$\mathbf{D}_{\tilde{\mathbf{x}}\tilde{\mathbf{x}}}^{(inv)} \triangleq \text{ddiag}(\mathbf{C}_{\tilde{\mathbf{x}}\tilde{\mathbf{x}}}^{-1}) \quad (18)$$

and

$$\mathbf{D}_{\tilde{\mathbf{w}}\tilde{\mathbf{w}}}^{(inv)} \triangleq \text{ddiag}(\mathbf{C}_{\tilde{\mathbf{w}}\tilde{\mathbf{w}}}^{-1}). \quad (19)$$

Similar to the derivations of (13) and (15), the minimization of  $Q_{freq}^{(d)}(\tilde{\mathbf{x}})$  from (10) w.r.t.  $\tilde{\mathbf{x}}$  by the Gauss-Newton method results in the following update equation:

$$\begin{aligned} \hat{\mathbf{x}}^{(t+1)} &= \hat{\mathbf{x}}^{(t)} \\ &\quad - \alpha^{(t)} \left( \mathbf{D}_{\hat{\mathbf{x}}\hat{\mathbf{x}}}^{(inv)} + \tilde{\mathbf{G}}(\mathbf{L}, \mathbf{V}\hat{\mathbf{x}}^{(t)})^T \mathbf{D}_{\tilde{\mathbf{w}}\tilde{\mathbf{w}}}^{(inv)} \tilde{\mathbf{G}}(\mathbf{L}, \mathbf{V}\hat{\mathbf{x}}^{(t)}) \right)^{-1} \\ &\quad \times \left( \mathbf{D}_{\hat{\mathbf{x}}\hat{\mathbf{x}}}^{(inv)} (\hat{\mathbf{x}}^{(t)} - \tilde{\boldsymbol{\mu}}_{\mathbf{x}}) \right. \\ &\quad \left. - \tilde{\mathbf{G}}(\mathbf{L}, \mathbf{V}\hat{\mathbf{x}}^{(t)})^T \mathbf{D}_{\tilde{\mathbf{w}}\tilde{\mathbf{w}}}^{(inv)} (\tilde{\mathbf{y}} - \tilde{\mathbf{g}}(\mathbf{L}, \mathbf{V}\hat{\mathbf{x}}^{(t)})) \right). \end{aligned} \quad (20)$$

That is, (17) is obtained by replacing the inverse of the full covariance matrices  $\mathbf{C}_{\tilde{\mathbf{x}}\tilde{\mathbf{x}}}$  and  $\mathbf{C}_{\tilde{\mathbf{w}}\tilde{\mathbf{w}}}^{-1}$  in (9) with diagonal versions in (18) and (19).

In Subsection IV-C, we present the orthogonal-graph-frequencies case, in which the estimator from (20) that minimizes the objective in (17) is separable in the graph-frequency domain and can be implemented with per-coordinate iterations. Thus, in this case, the estimator from (20) has a lower computational complexity than the MAP estimator. However, in the general case, a main problem is that the matrix  $\tilde{\mathbf{G}}(\mathbf{L}, \mathbf{V}\hat{\mathbf{x}}^{(t)})$  in (20) is a full matrix that changes at each iteration. To bypass this hurdle, we use the Gauss-Newton iteration in (20) with an additional step of neglecting the off-diagonal elements of  $\tilde{\mathbf{G}}(\mathbf{L}, \mathbf{V}\hat{\mathbf{x}}^{(t)})$ . This approach results in a separable form of the estimator in the graph-frequency domain for the general non-orthogonal case.

In the second step, at each iteration of (20) we neglect the non-diagonal elements of the Jacobian matrix,  $\tilde{\mathbf{G}}(\mathbf{L}, \mathbf{V}\hat{\mathbf{x}}^{(t)})$  that involves the mixed-derivatives of  $\tilde{\mathbf{g}}(\mathbf{L}, \mathbf{V}\hat{\mathbf{x}})$ . This results

in the following iteration:

$$\begin{aligned} \hat{\mathbf{x}}^{(t+1)} &= \hat{\mathbf{x}}^{(t)} - \alpha^{(t)} \left( \mathbf{D}_{\hat{\mathbf{x}}\hat{\mathbf{x}}}^{(inv)} + \mathbf{D}_{\tilde{\mathbf{w}}\tilde{\mathbf{w}}}^{(inv)} \bar{\mathbf{D}}_{\tilde{\mathbf{G}}\tilde{\mathbf{G}}}(\hat{\mathbf{x}}^{(t)})^2 \right)^{-1} \\ &\quad \times \left( \mathbf{D}_{\hat{\mathbf{x}}\hat{\mathbf{x}}}^{(inv)} (\hat{\mathbf{x}}^{(t)} - \tilde{\boldsymbol{\mu}}_{\mathbf{x}}) \right. \\ &\quad \left. - \mathbf{D}_{\tilde{\mathbf{w}}\tilde{\mathbf{w}}}^{(inv)} \bar{\mathbf{D}}_{\tilde{\mathbf{G}}\tilde{\mathbf{G}}}(\hat{\mathbf{x}}^{(t)}) (\tilde{\mathbf{y}} - \tilde{\mathbf{g}}(\mathbf{L}, \mathbf{V}\hat{\mathbf{x}}^{(t)})) \right), \end{aligned} \quad (21)$$

where

$$\bar{\mathbf{D}}_{\tilde{\mathbf{G}}\tilde{\mathbf{G}}}(\tilde{\mathbf{x}}) = \text{ddiag}(\tilde{\mathbf{G}}(\mathbf{L}, \mathbf{V}\tilde{\mathbf{x}})).$$

The estimator in (21) is denoted the eGFD-MAP estimator. The advantages of the eGFD-MAP estimator compared with the conventional MAP iterative methods from Subsection III-C are that: 1) there is no need to calculate the off-diagonal elements of the Jacobian matrix  $\tilde{\mathbf{G}}(\mathbf{L}, \mathbf{V}\tilde{\mathbf{x}})$  at each iteration; and 2) there is no need for performing matrix inversion per iteration. Indeed, in order to compute  $\mathbf{D}_{\hat{\mathbf{x}}\hat{\mathbf{x}}}^{(inv)}$  and  $\mathbf{D}_{\tilde{\mathbf{w}}\tilde{\mathbf{w}}}^{(inv)}$  there is a need to compute the inverse of the prior covariance matrices  $\mathbf{C}_{\tilde{\mathbf{x}}\tilde{\mathbf{x}}}$  and  $\mathbf{C}_{\tilde{\mathbf{w}}\tilde{\mathbf{w}}}$ . However, this calculation does not change at each iteration, and thus can be done offline where  $\mathbf{C}_{\tilde{\mathbf{x}}\tilde{\mathbf{x}}}$  and  $\mathbf{C}_{\tilde{\mathbf{w}}\tilde{\mathbf{w}}}$  are assumed to be known. In particular, assuming the covariance matrices and the Jacobian matrix are given, performing a single iteration of the MAP update equation according to (13) or (15) requires  $\mathcal{O}(N^3)$  calculations since, in general, there is a need for performing matrix inversion, while the update step of the eGFD-MAP from (21) requires only  $\mathcal{O}(N)$  calculations. Due to these two advantages, and the fact that (21) can be implemented in a component-wise fashion, the eGFD-MAP estimator in (21) can result in a significant overall speedup and can be used even when the size of the network is large, in contrast with the MAP estimator, which becomes intractable in large networks. In addition, in cases where the matrices  $\mathbf{C}_{\tilde{\mathbf{x}}\tilde{\mathbf{x}}}^{-1} + \mathbf{G}^T(\mathbf{L}, \hat{\mathbf{x}}^{(t)}) \mathbf{C}_{\tilde{\mathbf{w}}\tilde{\mathbf{w}}}^{-1} \mathbf{G}(\mathbf{L}, \hat{\mathbf{x}}^{(t)})$  in (13) or  $\mathbf{C}_{\tilde{\mathbf{x}}\tilde{\mathbf{x}}}^{-1} + \tilde{\mathbf{G}}^T(\mathbf{L}, \mathbf{V}\hat{\mathbf{x}}^{(t)}) \mathbf{C}_{\tilde{\mathbf{w}}\tilde{\mathbf{w}}}^{-1} \tilde{\mathbf{G}}(\mathbf{L}, \mathbf{V}\hat{\mathbf{x}}^{(t)})$  in (15), are ill-conditioned (as may happen when the sample covariance matrices are used instead of the true covariances), the calculation of their inverse is prone to large numerical errors. This can badly affect the performance of the MAP estimator, in contrast to the performance of the eGFD-MAP estimator that does not require matrix inversion. Finally, the eGFD-MAP-estimator algorithm is summarized in Algorithm 3.

### B. GSP-MAP estimator

While the eGFD-MAP estimator has a lower computational cost, it is an ad-hoc estimator. In this subsection, we aim to find an optimal approach in the GSP sense. As shown in Subsection III-C, the update equation of the MAP estimator is obtained by solving a linearized WLS problem at each iteration. As a result, the update equations under the three objective functions in (13), (15), and (21) are all linear functions of  $\mathbf{y} - \mathbf{g}(\mathbf{L}, \hat{\mathbf{x}}^{(t)})$  and of  $\hat{\mathbf{x}}^{(t)} - \boldsymbol{\mu}_{\mathbf{x}}$ . Based on this representation, in the following we remain with the linearized WLS problem but constrain the estimator at each iteration  $t$  to be the output of two graph filters.

In particular, in the following, we consider that at the  $t$ th iteration, the estimator has the form:

$$\begin{aligned} \hat{\mathbf{x}}^{(t+1)} &= \hat{\mathbf{x}}^{(t)} + f_1(\mathbf{L}, \hat{\mathbf{x}}^{(t)}) (\hat{\mathbf{x}}^{(t)} - \boldsymbol{\mu}_{\mathbf{x}}) \\ &\quad + f_2(\mathbf{L}, \hat{\mathbf{x}}^{(t)}) (\mathbf{y} - \mathbf{g}(\mathbf{L}, \hat{\mathbf{x}}^{(t)})), \end{aligned} \quad (22)$$

---

**Algorithm 3:** eGFD-MAP estimator by Gauss-Newton
 

---

**Input:**

- The function  $\tilde{\mathbf{g}}(\mathbf{L}, \mathbf{V}\hat{\mathbf{x}})$
- The Laplacian matrix  $\mathbf{L}$
- Initial step size  $\alpha^{(0)}$ ,  $\gamma$  and  $\Delta$
- The mean and the diagonal entries of the inverse covariance matrices:  $\tilde{\boldsymbol{\mu}}_{\mathbf{x}}$ ,  $\mathbf{D}_{\tilde{\mathbf{x}}\tilde{\mathbf{x}}}^{(\text{inv})}$ , and  $\mathbf{D}_{\tilde{\mathbf{w}}\tilde{\mathbf{w}}}^{(\text{inv})}$
- The tolerance  $\delta$

**Algorithm Steps:**

- 1) Initialization:  $\hat{\mathbf{x}}^{(0)}$
- 2) Compute  $\tilde{\mathbf{g}}(\mathbf{L}, \mathbf{V}\hat{\mathbf{x}}^{(t)})$  and  $\bar{\mathbf{D}}_{\tilde{\mathbf{G}}\tilde{\mathbf{G}}}(\hat{\mathbf{x}}^{(t)})$  from (16)
- 3) Choose step size  $\alpha^{(t)}$  according to Algorithm 2 with the cost  $Q_{freq}^{(d)}$  from (17)
- 4) Apply iteration step according to (21)
- 5) Stopping condition:  $\|\hat{\mathbf{x}}^{(t+1)} - \hat{\mathbf{x}}^{(t)}\| < \delta$

**Output:** eGFD-MAP estimator  $\hat{\mathbf{x}} = \mathbf{V}\hat{\mathbf{x}}^{(t+1)}$

---

where  $f_i(\cdot, \cdot)$ ,  $i = 1, 2$ , are graph filters as defined in (4). By left-multiplying (22) by  $\mathbf{V}^T$ , we obtain that in the graph domain representation the estimator from (22) can be written as

$$\begin{aligned} \hat{\mathbf{x}}^{(t+1)} &= \hat{\mathbf{x}}^{(t)} + f_1(\mathbf{A}, \mathbf{V}\hat{\mathbf{x}}^{(t)})(\hat{\mathbf{x}}^{(t)} - \tilde{\boldsymbol{\mu}}_{\mathbf{x}}) \\ &\quad + f_2(\mathbf{A}, \mathbf{V}\hat{\mathbf{x}}^{(t)})(\tilde{\mathbf{y}} - \tilde{\mathbf{g}}(\mathbf{L}, \mathbf{V}\hat{\mathbf{x}}^{(t)})), \end{aligned} \quad (23)$$

where  $\mathbf{V}$  and  $\mathbf{A}$  are the eigenvector-eigenvalue matrices of the Laplacian matrix,  $\mathbf{L}$ , as defined in (1).

In this form of estimators, the terms  $\hat{\mathbf{x}}^{(t)} - \tilde{\boldsymbol{\mu}}_{\mathbf{x}}$  and  $\tilde{\mathbf{y}} - \tilde{\mathbf{g}}(\mathbf{L}, \mathbf{V}\hat{\mathbf{x}}^{(t)})$  are multiplied by *diagonal* matrices that represent the graph filters. It can be seen that in the general case, the estimators in (13) and (15) cannot be written in the form of (22) or (23). In contrast, the iteration of the eGFD-MAP estimator from (21) can be written as the output of graph filters, as described in (23), where  $f_1(\cdot, \cdot)$  and  $f_2(\cdot, \cdot)$  are the following graph filters:

$$\begin{aligned} f_1^{\text{eGFD-MAP}}(\mathbf{A}, \mathbf{V}\hat{\mathbf{x}}^{(t)}) &= -\alpha^{(t)} \left( \mathbf{D}_{\tilde{\mathbf{x}}\tilde{\mathbf{x}}}^{(\text{inv})} + \mathbf{D}_{\tilde{\mathbf{w}}\tilde{\mathbf{w}}}^{(\text{inv})} \bar{\mathbf{D}}_{\tilde{\mathbf{G}}\tilde{\mathbf{G}}}^2(\hat{\mathbf{x}}^{(t)}) \right)^{-1} \mathbf{D}_{\tilde{\mathbf{x}}\tilde{\mathbf{x}}}^{(\text{inv})} \end{aligned} \quad (24)$$

and

$$\begin{aligned} f_2^{\text{eGFD-MAP}}(\mathbf{A}, \mathbf{V}\hat{\mathbf{x}}^{(t)}) &= \alpha^{(t)} \\ &\times \left( \mathbf{D}_{\tilde{\mathbf{x}}\tilde{\mathbf{x}}}^{(\text{inv})} + \mathbf{D}_{\tilde{\mathbf{w}}\tilde{\mathbf{w}}}^{(\text{inv})} \bar{\mathbf{D}}_{\tilde{\mathbf{G}}\tilde{\mathbf{G}}}^2(\hat{\mathbf{x}}^{(t)}) \right)^{-1} \mathbf{D}_{\tilde{\mathbf{w}}\tilde{\mathbf{w}}}^{(\text{inv})} \bar{\mathbf{D}}_{\tilde{\mathbf{G}}\tilde{\mathbf{G}}}(\hat{\mathbf{x}}^{(t)}). \end{aligned} \quad (25)$$

In the following, our goal is to choose the graph filters  $f_1(\cdot, \cdot)$  and  $f_2(\cdot, \cdot)$  in the updated equation in (22) (or, equivalently, in (23)) in an optimal way in the sense that the expected objective function  $Q_{lin}$  from (12) is minimized for the general case. It should be noted that the graph filters can be a function of the previous-iteration estimator,  $\hat{\mathbf{x}}^{(t)}$ . The following theorem describes the MAP-optimal graph filters.

**Theorem 1.** *The graph filters that minimize the expected objective function,*

$$\mathbb{E} \left[ Q_{lin}(\hat{\mathbf{x}}^{(t+1)}, \hat{\mathbf{x}}^{(t)}) \Big| \hat{\mathbf{x}}^{(t)} = \mathbf{x} \right], \quad (26)$$

over the subset of GSP estimators defined in (22), under the approximation that  $\tilde{\mathbf{G}}(\mathbf{L}, \mathbf{V}\hat{\mathbf{x}}^{(t)})$  is a deterministic matrix<sup>1</sup>, are

$$\begin{aligned} f_1^*(\mathbf{A}, \hat{\mathbf{x}}^{(t)}) &= -\text{diag} \left( \left( \mathbf{C}_{\tilde{\mathbf{x}}\tilde{\mathbf{x}}} \circ \mathbf{C}_{\tilde{\mathbf{x}}\tilde{\mathbf{x}}}^{-1} \right. \right. \\ &\quad \left. \left. + \mathbf{C}_{\tilde{\mathbf{x}}\tilde{\mathbf{x}}} \circ (\tilde{\mathbf{G}}^T(\mathbf{L}, \mathbf{V}\hat{\mathbf{x}}^{(t)}) \mathbf{C}_{\tilde{\mathbf{w}}\tilde{\mathbf{w}}}^{-1} \tilde{\mathbf{G}}(\mathbf{L}, \mathbf{V}\hat{\mathbf{x}}^{(t)})) \right)^{-1} \mathbf{1} \right) \end{aligned} \quad (27)$$

and

$$\begin{aligned} f_2^*(\mathbf{A}, \hat{\mathbf{x}}^{(t)}) &= \text{diag} \left( \left( \mathbf{C}_{\tilde{\mathbf{w}}\tilde{\mathbf{w}}} \circ \mathbf{C}_{\tilde{\mathbf{w}}\tilde{\mathbf{w}}}^{-1} \right. \right. \\ &\quad \left. \left. + \mathbf{C}_{\tilde{\mathbf{w}}\tilde{\mathbf{w}}} \circ (\tilde{\mathbf{G}}^T(\mathbf{L}, \mathbf{V}\hat{\mathbf{x}}^{(t)}) \mathbf{C}_{\tilde{\mathbf{w}}\tilde{\mathbf{w}}}^{-1} \tilde{\mathbf{G}}(\mathbf{L}, \mathbf{V}\hat{\mathbf{x}}^{(t)})) \right)^{-1} \right. \\ &\quad \left. \times \text{diag}(\tilde{\mathbf{G}}(\mathbf{L}, \mathbf{V}\hat{\mathbf{x}}^{(t)})) \right) \end{aligned} \quad (28)$$

at the  $t+1$  iteration.

*Proof:* The full proof appears in Appendix B. The main course of the proof is composed of two steps; in the first step, it is shown that under the theorem conditions, we can replace the minimization of (26) by the minimization of

$$\begin{aligned} \mathbb{E}[Q_{lin}^{approx}(\tilde{\mathbf{x}}, \hat{\mathbf{x}}^{(t)})] &= \frac{1}{2} \text{trace}(\mathbf{C}_{\tilde{\mathbf{x}}\tilde{\mathbf{x}}}(\mathbf{I} + f_1(\mathbf{A})) \mathbf{C}_{\tilde{\mathbf{x}}\tilde{\mathbf{x}}}^{-1}((\mathbf{I} + f_1(\mathbf{A}))) \\ &\quad + \frac{1}{2} \text{trace}(\mathbf{C}_{\tilde{\mathbf{w}}\tilde{\mathbf{w}}} f_2(\mathbf{A}) \mathbf{C}_{\tilde{\mathbf{x}}\tilde{\mathbf{x}}}^{-1} f_2(\mathbf{A})) \\ &\quad + \frac{1}{2} \text{trace}(\mathbf{C}_{\tilde{\mathbf{x}}\tilde{\mathbf{x}}} f_1(\mathbf{A}) \mathbf{A} f_1(\mathbf{A})) \\ &\quad + \text{trace} \left( \frac{1}{2} \mathbf{I} - \tilde{\mathbf{G}}(\mathbf{L}, \mathbf{V}\hat{\mathbf{x}}^{(t)}) f_2(\mathbf{A}) \right) \\ &\quad + \frac{1}{2} \text{trace}(\mathbf{C}_{\tilde{\mathbf{w}}\tilde{\mathbf{w}}} f_2(\mathbf{A}) \mathbf{A} f_2(\mathbf{A})), \end{aligned} \quad (29)$$

where  $\mathcal{D}_N$  is the set of diagonal matrices of size  $N \times N$  and

$$\mathbf{A} \triangleq \tilde{\mathbf{G}}^T(\mathbf{L}, \mathbf{V}\hat{\mathbf{x}}^{(t)}) \mathbf{C}_{\tilde{\mathbf{w}}\tilde{\mathbf{w}}}^{-1} \tilde{\mathbf{G}}(\mathbf{L}, \mathbf{V}\hat{\mathbf{x}}^{(t)}). \quad (30)$$

Then, in the second step, it is shown that this minimization w.r.t. the graph filters results in (27) and (28). ■

Similar to the iterative algorithms from Section III-C, in practice, we multiply these graph filters by the step size  $\alpha^{(t)} \in (0, 1]$  that is computed by a backtracking line search. The GSP-MAP algorithm is summarized in Algorithm 4.

### C. Orthogonal-graph-frequencies models

In this subsection, we present the special case of orthogonal graph frequencies, and its special case in which the measured graph signal is the output of a GSP filter. We show that in the case of orthogonal graph frequencies, the proposed eGFD-MAP and GSP-MAP estimators coincide with the MAP estimator.

The orthogonal-graph-frequencies model is defined as follows.

**Definition 1.** *The nonlinear measurements function,  $\mathbf{g}(\mathbf{L}, \mathbf{x}) \in \mathbb{R}^N$ , is separable in the graph-frequency domain (“orthogonal graph frequencies”) if it satisfies*

$$[\tilde{\mathbf{g}}(\mathbf{L}, \mathbf{V}\tilde{\mathbf{x}})]_n = [\tilde{\mathbf{g}}(\mathbf{L}, \tilde{x}_n \mathbf{v}_n)]_n, \quad n = 1, \dots, N, \quad (32)$$

<sup>1</sup>The rationale behind this approximation is similar to that behind the first-order approximation in the Gauss-Newton method [40].

**Algorithm 4:** GSP-MAP estimator by Gauss-Newton**Input:**

- The function  $\tilde{\mathbf{g}}(\mathbf{L}, \mathbf{V}\tilde{\mathbf{x}})$
- The Laplacian matrix  $\mathbf{L}$
- Initial step size  $\alpha^{(0)}$ ,  $\gamma$  and  $\Delta$
- The mean and covariance matrices  $\tilde{\boldsymbol{\mu}}_{\mathbf{x}}$ ,  $\mathbf{C}_{\tilde{\mathbf{x}}\tilde{\mathbf{x}}}$ , and  $\mathbf{C}_{\tilde{\mathbf{w}}\tilde{\mathbf{w}}}$
- The tolerance  $\delta$

**Algorithm Steps:**

- 1) Initialization:  $\hat{\tilde{\mathbf{x}}}^{(0)}$
- 2) Compute  $\tilde{\mathbf{g}}(\mathbf{L}, \mathbf{V}\hat{\tilde{\mathbf{x}}}^{(t)})$  and  $\tilde{\mathbf{G}}(\mathbf{L}, \mathbf{V}\hat{\tilde{\mathbf{x}}}^{(t)})$  from (16)
- 3) Compute the graph filters  $f_1^*(\boldsymbol{\Lambda}, \hat{\tilde{\mathbf{x}}}^{(t)})$  and  $f_2^*(\boldsymbol{\Lambda}, \hat{\tilde{\mathbf{x}}}^{(t)})$  from (28) and (27)
- 4) Choose step size  $\alpha^{(t)}$  according to Algorithm 2 with the cost  $Q_{freq}$ .
- 5) Apply iteration step based on (23) with the computed graph filters:
 
$$\hat{\tilde{\mathbf{x}}}^{(t+1)} = \hat{\tilde{\mathbf{x}}}^{(t)} + \alpha^{(t)} f_1^*(\boldsymbol{\Lambda}, \mathbf{V}\hat{\tilde{\mathbf{x}}}^{(t)}) (\hat{\tilde{\mathbf{x}}}^{(t)} - \tilde{\boldsymbol{\mu}}_{\mathbf{x}}) + \alpha^{(t)} f_2^*(\boldsymbol{\Lambda}, \mathbf{V}\hat{\tilde{\mathbf{x}}}^{(t)}) (\tilde{\mathbf{y}} - \tilde{\mathbf{g}}(\mathbf{L}, \mathbf{V}\hat{\tilde{\mathbf{x}}}^{(t)})) \quad (31)$$
- 6) Stopping condition:  $\|\hat{\tilde{\mathbf{x}}}^{(t+1)} - \hat{\tilde{\mathbf{x}}}^{(t)}\| < \delta$

**Output:** Graph-filtered GSP-MAP estimator  $\hat{\tilde{\mathbf{x}}} = \mathbf{V}\hat{\tilde{\mathbf{x}}}^{(t+1)}$ 

where  $\tilde{x}_n$  is the  $n$ th element of  $\tilde{\mathbf{x}}$  and  $\tilde{\mathbf{g}}(\mathbf{L}, \mathbf{V}\tilde{\mathbf{x}}) = \mathbf{V}^T \mathbf{g}(\mathbf{L}, \mathbf{x})$ .

Definition 1 is satisfied, for example, if the associated Jacobian matrix,  $\mathbf{G}(\mathbf{L}, \mathbf{x})$ , is diagonalized by the eigenvector matrix of  $\mathbf{L}$ ,  $\mathbf{V}$ .

By substituting (32) in (17), we obtain that in this case

$$Q_{freq}^{(d)}(\tilde{\mathbf{x}}) = \frac{1}{2} \sum_{n=1}^N (\tilde{x}_n - [\tilde{\boldsymbol{\mu}}_{\mathbf{x}}]_n)^2 [\mathbf{C}_{\tilde{\mathbf{x}}\tilde{\mathbf{x}}}^{-1}]_{n,n} + \frac{1}{2} \sum_{n=1}^N (\tilde{y}_n - [\tilde{\mathbf{g}}(\mathbf{L}, \tilde{x}_n \mathbf{v}_n)]_n)^2 [\mathbf{C}_{\tilde{\mathbf{w}}\tilde{\mathbf{w}}}^{-1}]_{n,n}. \quad (33)$$

Thus, in the case described by Definition 1, the objective  $Q_{freq}^{(d)}(\tilde{\mathbf{x}})$  is separable in the graph-frequency domain. The component-wise formulation of (33) results in a separable nonlinear WLS problem [41], which simplifies the task of designing the MAP estimator in the graph-frequency domain without the need for neglecting off-diagonal elements (as performed in the eGFD-MAP estimator). The minimization of (33) instead of (9) results in  $N$  independent optimization problems that can result in an overall significant speedup. Minimization of (33) can be simplified even further if the graph input signal is a graph-bandlimited signal as defined in (3). In this case, by substituting  $\tilde{x}_n = 0, \forall n > N_s$ , the sums in (33) can be computed only over  $n = 1, \dots, N_s$ .

The following theorem states sufficient conditions for the proposed eGFD-MAP and GSP-MAP estimators to coincide with the MAP estimator for the case of an orthogonal-graph frequencies.

**Theorem 2.** *If the measurement function satisfies Definition 1 and, in addition, the following conditions hold:*

- C.1) *The elements of the input graph signal,  $\mathbf{x}$ , are statistically independent in the graph-frequency domain, i.e.*

*$\mathbf{C}_{\tilde{\mathbf{x}}\tilde{\mathbf{x}}}$  is a diagonal matrix;*

- C.2) *The noise vector,  $\mathbf{w}$ , is uncorrelated in the graph-frequency domain, i.e.  $\mathbf{C}_{\tilde{\mathbf{w}}\tilde{\mathbf{w}}}$  is a diagonal matrix;*  
*then, the proposed eGFD-MAP and GSP-MAP estimators coincide with the MAP estimator.*

*Proof:* By substituting (32), together with  $\mathbf{C}_{\tilde{\mathbf{w}}\tilde{\mathbf{w}}}^{-1} = \mathbf{D}_{\tilde{\mathbf{w}}\tilde{\mathbf{w}}}^{(inv)}$  and  $\mathbf{C}_{\tilde{\mathbf{x}}\tilde{\mathbf{x}}}^{-1} = \mathbf{D}_{\tilde{\mathbf{x}}\tilde{\mathbf{x}}}^{(inv)}$  from Conditions C.1 and C.2, respectively, in the MAP objective function in the graph-frequency domain in (9), we obtain that in this case

$$Q_{freq}(\tilde{\mathbf{x}}) = \frac{1}{2} (\tilde{\mathbf{x}} - \tilde{\boldsymbol{\mu}}_{\mathbf{x}})^T \mathbf{D}_{\tilde{\mathbf{x}}\tilde{\mathbf{x}}}^{(inv)} (\tilde{\mathbf{x}} - \tilde{\boldsymbol{\mu}}_{\mathbf{x}}) + \frac{1}{2} (\tilde{\mathbf{y}} - \tilde{\mathbf{g}}(\mathbf{L}, \mathbf{x}))^T \mathbf{D}_{\tilde{\mathbf{w}}\tilde{\mathbf{w}}}^{(inv)} (\tilde{\mathbf{y}} - \tilde{\mathbf{g}}(\mathbf{L}, \mathbf{V}\tilde{\mathbf{x}})) = \frac{1}{2} \sum_{n=1}^N (\tilde{x}_n - [\tilde{\boldsymbol{\mu}}_{\mathbf{x}}]_n)^2 [\mathbf{C}_{\tilde{\mathbf{x}}\tilde{\mathbf{x}}}^{-1}]_{n,n} + \frac{1}{2} \sum_{n=1}^N (\tilde{y}_n - [\tilde{\mathbf{g}}(\mathbf{L}, \tilde{x}_n \mathbf{v}_n)]_n)^2 [\mathbf{C}_{\tilde{\mathbf{w}}\tilde{\mathbf{w}}}^{-1}]_{n,n}. \quad (34)$$

Thus, the eGFD-MAP objective from (33) coincides with the MAP objective from (34). From Definition 1, we have that  $\tilde{\mathbf{G}}(\mathbf{L}, \mathbf{V}\tilde{\mathbf{x}}) = \bar{\mathbf{D}}_{\tilde{\mathbf{G}}\tilde{\mathbf{G}}}(\tilde{\mathbf{x}})$ . Therefore, we can conclude that the eGFD-MAP estimator coincides with the MAP estimator. By substituting,  $\mathbf{C}_{\tilde{\mathbf{x}}\tilde{\mathbf{x}}}^{-1} = \mathbf{D}_{\tilde{\mathbf{x}}\tilde{\mathbf{x}}}^{(inv)}$ ,  $\mathbf{C}_{\tilde{\mathbf{w}}\tilde{\mathbf{w}}}^{-1} = \mathbf{D}_{\tilde{\mathbf{w}}\tilde{\mathbf{w}}}^{(inv)}$ , and  $\tilde{\mathbf{G}}(\mathbf{L}, \mathbf{V}\hat{\tilde{\mathbf{x}}}^{(t)}) = \bar{\mathbf{D}}_{\tilde{\mathbf{G}}\tilde{\mathbf{G}}}(\hat{\tilde{\mathbf{x}}}^{(t)})$  in the optimal graph filters from (27) and (28), and using the fact that  $\mathbf{I} \circ \mathbf{A} = \text{ddiag}(\mathbf{A})$ ,  $\text{diag}(\mathbf{D}\mathbf{a}) = \mathbf{D}\text{diag}(\mathbf{a})$ , and  $\text{ddiag}(\mathbf{D}) = \mathbf{D}$  for any matrix  $\mathbf{A}$ , diagonal matrix,  $\mathbf{D}$ , and vector  $\mathbf{a}$ , we obtain the graph filters of the eGFD-MAP estimator from (24) and (25). Thus, the GSP-MAP estimator coincides with the eGFD-MAP estimator, which is also the MAP estimator. ■

The following corollary presents a special case of Theorem 2.

**Corollary 1.** *The proposed eGFD-MAP and GSP-MAP estimators coincide with the MAP estimator if Conditions C.1 and C.2 hold, and*

- C.3) *The measurement function,  $\mathbf{g}(\mathbf{L}, \mathbf{x})$ , is the output of a linear graph filter as defined in (4), i.e.*

$$\mathbf{g}(\mathbf{L}, \mathbf{x}) = \mathbf{V}f(\boldsymbol{\Lambda})\mathbf{V}^T\mathbf{x}. \quad (35)$$

*Proof:* By multiplying (35) by  $\mathbf{V}^T$  and using the fact that  $\mathbf{V}$  is unitary matrix, i.e.  $\mathbf{V}\mathbf{V}^T = \mathbf{I}$ , we obtain

$$\tilde{\mathbf{g}}(\mathbf{L}, \mathbf{V}\tilde{\mathbf{x}}) = f(\boldsymbol{\Lambda})\tilde{\mathbf{x}}. \quad (36)$$

Since  $f(\boldsymbol{\Lambda})$  is a diagonal matrix, we obtain that the measurement function satisfies (32) in Definition 1. Since, in addition, we assume that Conditions C.1 and C.2 of Theorem 2 hold, we obtain that this is a special case of Theorem 2. Thus, the eGFD-MAP and GSP-MAP estimators coincide with the MAP estimator in this case. ■

The special case in Corollary 1 fits the model behind the graphical Wiener filter [27], as explained in [18], where under Condition C.1, the signal  $\mathbf{x} - \mathbb{E}[\mathbf{x}]$  is a Graph Wide-Sense Stationary signal (see Definition 3 and Theorem 1 in [27]). Therefore, in the case where the conditions of Corollary 1 hold, an estimator that is obtained by minimizing (33) coincides with the graphical Wiener filter (Eq. (13) in [27]), the

MAP estimator, the LMMSE estimator, and the GSP-LMMSE estimator from [18]. In this case, the Gauss-Newton iterative approach converges in single iteration with a step size equal to 1, since  $\mathbf{g}$  is a linear function (see Sec. 1.5.1 in [37]).

#### D. Computational complexity

The computational complexity and the running time of the proposed iterative estimators mainly depend on: 1) the total number of iterations until convergence of the estimator; 2) the total subiterations in the backtracking line search algorithm (Algorithm 2); and 3) the matrix multiplications in the update step. If we assume that 1) and 2) are roughly similar among the different estimators (given that the parameters  $\alpha^{(0)}$ ,  $\gamma$ ,  $\Delta$ , and  $\delta$  are the same among the estimators), then the differences in the complexity and running time are due to the update steps of the different estimators. In addition, the computations of the inverse covariance matrices of  $\mathbf{x}$  and  $\mathbf{w}$  in the graph and graph-frequency domains, and the computation of the eigenvalue decomposition of the Laplacian matrix, which is of order  $\mathcal{O}(N^3)$ , can be done offline. Therefore, we do not consider them in the computational complexity.

The update rule of the MAP estimator in (13) consists of full matrix multiplications with a computational complexity of  $\mathcal{O}(N^3)$ , and inversion of an  $N \times N$  full matrix, which has a complexity of  $\mathcal{O}(N^3)$ . This also holds for the implementation of the MAP estimator in the graph-frequency domain; however, as mentioned, one implementation of the MAP (in the graph or graph-frequency domain) may be more efficient than the second one. The computational complexity of the update step of the GSP-MAP estimator is similar to that of the MAP estimator, since the reconstruction of each filter in (27) and (28) demands full matrix multiplications in the order of  $\mathcal{O}(N^3)$ , and inversion of a  $N \times N$  matrix. The update step of the eGFD-MAP estimator in (21) can be implemented in a vectorized form, and thus requires only  $\mathcal{O}(N)$  multiplications, without the need to invert a matrix. In addition, in order to perform the update steps of the MAP and GSP-MAP estimators, it is necessary to calculate  $N^2$  elements of the Jacobian matrix in (11) (or in (16)), compared to  $N$  diagonal elements for the eGFD-MAP estimator in (21). As the size of the network increases, the differences in the computational complexities of the estimators become more significant, so that in very large networks the MAP and GSP-MAP estimators may become intractable. The total floating point operations order of the update steps of the different estimators is summarized in Table I.

Estimator	MAP	eGFD-MAP	GSP-MAP
FLOPs	$11N^3 + 2.5N^2 + 1.5N$	$11N$	$10N^3 + 6.5N^2 + 5.5N$
Order	$\mathcal{O}(N^3)$	$\mathcal{O}(N)$	$\mathcal{O}(N^3)$

TABLE I: The total floating point operations (FLOPs) and order of complexity required for the update rules of the different estimators.

## V. SIMULATION

In this section, we evaluate the performance of the different estimators for a synthetic example in Subsection V-A and for

the PSSE problem in Subsection V-B. The estimators that are used in this section are:

- MAP estimator, implemented by Algorithm 1;
- MAP estimator in the graph-frequency domain (MAP-FD), implemented by Algorithm 1 while using (15);
- eGFD-MAP estimator, implemented by Algorithm 3;
- GSP-MAP estimator implemented by Algorithm 4;
- LMMSE estimator and GSP-LMMSE estimator from [18]; In Subsection V-A, the analytic-version of LMMSE and GSP-LMMSE estimators is implemented, while in Subsection V-B these estimators are implemented by their sample-mean version (i.e. where the intractable covariance matrices are replaced by the sample covariance matrices), as discussed in detail in [18]. Here, we used  $P = 500$  training samples to compute the sample covariance matrices.

All iterative estimators (MAP, eGFD-MAP, and GSP-MAP) were initialized by the GSP-LMMSE estimator, unless written otherwise. The performance of the different estimators is calculated by performing 10,000 Monte Carlo simulations for each scenario.

#### A. Example A: Synthetic data - orthogonal graph frequencies

In this example we use random graphs that were generated by the Watts-Strogatz small-world graph model [42], with different number of vertices,  $N$ , and a mean degree of  $K = 5$ . We evaluate the different estimators under the model from (5) with the following nonlinear measurement function in the graph-frequency domain:

$$[\tilde{\mathbf{g}}(\mathbf{L}, \mathbf{V}\tilde{\mathbf{x}})]_n = \tilde{\mathbf{x}}_n^3 \quad n = 1, \dots, N. \quad (37)$$

We assume that the *a-priori* pdf of  $\tilde{\mathbf{x}}$  is given by  $\tilde{\mathbf{x}} \sim \mathcal{N}(\mathbf{0}, \sigma_{\tilde{\mathbf{x}}}^2 \mathbf{I})$ . The noise  $\mathbf{w}$  from (5) is white Gaussian noise with  $\mathbf{C}_{\mathbf{w}\mathbf{w}} = \sigma_{\mathbf{w}}^2 \mathbf{I}$ . In the simulations, we use  $\sigma_{\tilde{\mathbf{x}}}^2 = 0.5$  and  $\sigma_{\mathbf{w}}^2 = 0.05$ . It can be verified that this nonlinear model has “orthogonal graph frequencies”, as defined in Definition 1, and that the conditions of Theorem 2 are satisfied since  $\tilde{\mathbf{x}}$  and  $\tilde{\mathbf{w}}$  are white Gaussian noise signals. Thus, according to Theorem 2 the MAP estimator coincides with the eGFD-MAP and the GSP-MAP estimators. Under this setting, the LMMSE and GSP-LMMSE estimators coincide and can be computed analytically by using  $\mathbf{C}_{\mathbf{y}\mathbf{y}} = (\sigma_{\mathbf{w}}^2 + 15\sigma_{\tilde{\mathbf{x}}}^6)\mathbf{I}$  and  $\mathbf{C}_{\mathbf{x}\mathbf{y}} = 3\sigma_{\tilde{\mathbf{x}}}^4 \mathbf{I}$ . In the simulations in this subsection, we also add the MAP-FD estimator in order to have a fair comparison in terms of run-time.

In Fig. 1 we present the normalized MSE (NMSE), i.e. the MSE divided by the number of vertices,  $N$ , of the different estimators versus  $N$ . In this case, the nonlinear estimators (MAP, MAP-FD, eGFD-MAP, and GSP-MAP estimators) significantly outperform the linear estimators (LMMSE and GSP-LMMSE), which have an almost constant NMSE for any  $N$  around the value 0.208 with a standard deviation of 0.001. Therefore, and due to resolution reasons, the linear estimators are omitted from this figure. Since in this case the conditions of Theorem 2 are satisfied, the MSEs of the nonlinear estimators (MAP, MAP-FD, eGFD-MAP, and GSP-MAP estimators) are all equal as expected from Theorem 2. It can be seen that the MSE of the nonlinear estimators increases as  $N$  increases. In Fig. 2 we present the averaged runtime of any estimator till



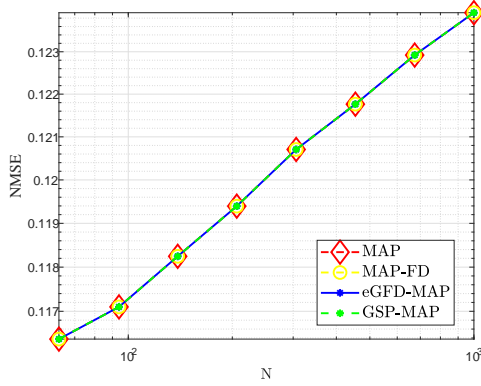


Fig. 1: Example A: The NMSE of the different estimators versus  $N$ .

convergence versus  $N$ , which is evaluated using MATLAB on an Intel Core(TM) i7-7500U CPU computer, 2.7 GHz. It can be seen that the eGFD-MAP estimator, which does not require matrix inversion per iteration, has the smallest runtime. This complexity reduction (in terms of run-time) becomes more evident as the dimension of the network increases. Hence the eGFD-MAP estimator is a good alternative to the MAP estimator in the cases where the measurement function is close to separable in the graph-frequency domain, i.e. has almost “orthogonal frequencies”. In addition, it can be seen that in this case, implementation in the graph frequency domain has lower computational complexity; indeed, the run-time of the MAP-FD estimator is lower than the run-time of the MAP estimator. The averaged run-time of the linear estimators (not shown in this figure due to resolution reasons) is significantly smaller than the iterative estimators (around  $1 \cdot 10^{-6}$  [sec]). This runtime would significantly increase in complex models where there is a need to compute the sample covariance matrices, as in the following subsection.

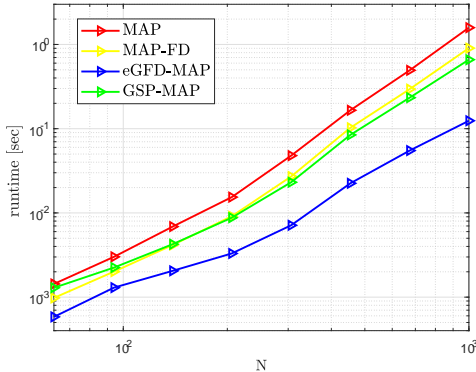


Fig. 2: Example A: The time complexity of the different estimators versus  $N$ .

### B. Example B: PSSE in electrical networks

A power system can be represented as an undirected weighted graph,  $\mathcal{G}(\mathcal{V}, \xi)$ , where the set of vertices,  $\mathcal{V}$ , is the set of buses (generators or loads) and the edge set,  $\xi$ , is the set

of transmission lines between these buses. The measurement vector of the active powers at the buses,  $\mathbf{y}$ , can be described by the model in (5) with the measurement function [43]:

$$[\mathbf{g}(\mathbf{L}, \mathbf{x})]_n \triangleq \sum_{m=1}^N |v_n||v_m|(G_{n,m} \cos(x_n - x_m) + B_{n,m} \sin(x_n - x_m)), \quad (38)$$

$n = 1, \dots, N$ . Here,  $x_n$  and  $|v_n|$  are the voltage phase and amplitude at the  $n$ th bus, and  $G_{n,m}$  and  $B_{n,m}$  are the conductance and susceptance of the transmission line between the buses  $n$  and  $m$  [43], where  $(n, m) \in \xi$ . We assume that  $|v_n| = 1$ , which is a common assumption in normalized power systems [43], and that  $G_{n,m}$  and  $B_{n,m}$  are all known. In the graph modeling of the electrical network, usually the Laplacian matrix,  $\mathbf{L}$ , is constructed as follows (Subsection II-C in [13]):

$$\mathbf{L} = \begin{cases} -B_{n,k}, & k \neq n \\ \sum_{\substack{m=1 \\ m \neq n}}^N B_{n,m}, & k = n. \end{cases} \quad (39)$$

The goal of PSSE is to recover the state vector,  $\mathbf{x}$ , from the power measurements,  $\mathbf{y}$ , described by (5) with the nonlinear measurement function  $\mathbf{g}(\mathbf{L}, \mathbf{x})$  in (38). This estimation task is known to be a NP-hard problem [44], and is essential for various monitoring purposes [43]. PSSE is traditionally solved by iterative methods, such as the Gauss-Newton method [43]. By substituting (38) in (11), we obtain that the associated Jacobian matrix is

$$[\mathbf{G}(\mathbf{L}, \mathbf{x})]_{n,k} = \frac{\partial \mathbf{g}_n(\mathbf{L}, \mathbf{x})}{\partial x_k} = \begin{cases} G_{n,k} \sin(x_n - x_k) - B_{n,k} \cos(x_n - x_k), & k \neq n \\ \sum_{\substack{m=1 \\ m \neq n}}^N -G_{n,m} \sin(x_n - x_m) + B_{n,m} \cos(x_n - x_m), & k = n \end{cases} \quad (40)$$

In particular, since  $G_{n,k} = 0$  and  $B_{n,k} = 0$  for any  $(n, k) \notin \xi$ , it can be seen that  $[\mathbf{G}(\mathbf{L}, \mathbf{x})]_{n,k} = 0$  for any  $(n, k) \notin \xi$ . It should be noted that in the general case, (40) implies that the conditions of Theorem 2 are not satisfied in this case.

The input graph signal,  $\mathbf{x}$ , has been shown to be smooth w.r.t. the graph [12], [45]. Therefore, we model the distribution of  $\mathbf{x}$  in the graph-frequency domain as a smooth, normal distribution [46], [47], as defined in (47) in Appendix A. Since in this case study,  $\mathbf{x}$  represents phases, the value of  $\beta$  in (47) is taken such that the probability that the elements of  $|\mathbf{x}|$  are larger than  $\pi$  is smaller than 0.01. We assume that the covariance matrix of the noise,  $\mathbf{w}$ , from the model in (5) is  $\mathbf{C}_{\mathbf{w}\mathbf{w}} = \sigma_{\mathbf{w}}^2 \mathbf{I}$ . The values of the different physical parameters in (38) are taken from the IEEE 118-bus test case [48], in which  $N = 118$ . In Table II we present the hyperparameters used to evaluate the different estimators in this and in the following subsections.

Finally, it can be seen that in the model in (38) there is an inherent ambiguity, and one can recover the phases in  $\mathbf{x}$  only up to modulo  $2\pi$  errors. Therefore, in the following simulations, the error is presented in terms of mean-squared-periodic-error (MSPE) [49]:

$$\text{MSPE}(\mathbf{x}, \hat{\mathbf{x}}) = \mathbb{E} \left[ (\text{mod}_{2\pi}(\mathbf{x} - \hat{\mathbf{x}}))^2 \right], \quad (41)$$

Estimator	MAP	eGFD-MAP	GSP-MAP
$\alpha_0$	0.5	0.5	0.5
$\gamma$	0.83	0.83	0.83
$\delta$	0.1	0.1	0.1
$\Delta$	0.01	0.01	0.01

TABLE II: The hyperparameters used for the simulations in Subsections V-B and V-C.

where  $\text{mod}_\pi$  denotes the element-wise modulo operator. The units of the MSPE are  $[\text{rad}^2]$ . The normalized MSPE (NMSPE) is obtained by dividing the MSPE by  $N$ .

In Fig. 3 we present the NMSPE of the different estimators versus the inverse of the noise variance,  $\frac{1}{\sigma_w^2}$ , for the 118-bus case. It can be seen that the MAP, eGFD-MAP, and GSP-MAP estimators significantly outperform the linear estimators (LMMSE and GSP-LMMSE estimators) in terms of MSPE for  $\sigma_w^2 < 1$ . As the noise variance,  $\sigma_w^2$ , increases, the MSPE of the LMMSE and the GSP-LMMSE achieved the MSPE of the nonlinear estimators, since in the presence of significant measurement noise, all estimators are reduced to the prior-mean estimator,  $\mu_x$ , which is a linear estimator. Therefore, this figure shows that we can achieve good performance with the low-complexity eGFD-MAP estimator and with the GSP-MAP estimator even when the measurement function does not have orthogonal graph frequencies. In addition, the proposed estimators has a lower MSPE than the MAP estimator for large noise variance, since they have fewer parameters to determine. Thus, in this case, the proposed methods are more robust to noise than the MAP estimator.

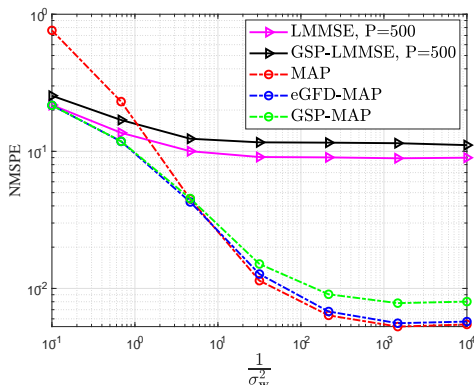


Fig. 3: The NMSPE of the different estimators versus  $\frac{1}{\sigma_w^2}$  for 118-bus test case with  $\beta = 3$ .

In order to examine the robustness of the iterative estimators under different phase distributions, and in particular under different levels of separability of the measurement function, we changed the value of  $\beta$  from (47), which directly affects the separability of the measurement function in the sense of Definition 1. As  $\beta$  increases, the total variation of the signal  $\mathbf{x}$ , which is defined as  $\mathbf{x}^T \mathbf{L} \mathbf{x}$ , increases. From the distribution in (47), and recalling that  $\mathbf{x} = \mathbf{V} \tilde{\mathbf{x}}$ , the variance of  $x_i$  can be expressed as

$$\text{var}(x_i) = \beta \sum_{j=1}^N \frac{V_{i,j}^2}{\lambda_j}. \quad (42)$$

Thus, as  $\beta$  decreases, the phases are more concentrated around

their mean, which is assumed to be the same for any  $n = 1, \dots, N$ . Hence, as  $\beta$  decreases the difference  $x_n - x_m$  is smaller and when it is sufficiently small it is possible to use the first order Taylor approximation:

$$\sin(x_n - x_m) \approx x_n - x_m, \quad \cos(x_n - x_m) \approx 1 \quad (43)$$

Therefore, by substituting (43) in (38) and taking the derivative w.r.t  $\mathbf{x}$ , we obtain that the Jacobian of  $\mathbf{g}(\mathbf{L}, \mathbf{x})$  from (38) can be approximated by

$$\mathbf{G}(\mathbf{L}, \mathbf{x}) \approx -\mathbf{L} = \mathbf{V} \mathbf{\Lambda} \mathbf{V}^T, \quad (44)$$

where we used (39) and the eigenvalue decomposition of  $\mathbf{L}$ . By multiplying (44) by  $\mathbf{V}^T$  and  $\mathbf{V}$  from the left and right, respectively, and by using (16), one obtains

$$\tilde{\mathbf{G}}(\mathbf{L}, \mathbf{V} \tilde{\mathbf{x}}) \approx -\mathbf{\Lambda}, \quad (45)$$

i.e.  $\tilde{\mathbf{G}}(\mathbf{L}, \mathbf{V} \tilde{\mathbf{x}})$  is a diagonal matrix. Equation (45) implies that as  $\beta$  decreases,  $\tilde{\mathbf{g}}(\mathbf{L}, \mathbf{V} \tilde{\mathbf{x}})$  becomes more separable in the sense of Definition 1. However, for a general  $\beta$ ,  $\tilde{\mathbf{g}}(\mathbf{L}, \mathbf{V} \tilde{\mathbf{x}})$  may not be separable as required by Definition 1 (or, equivalently  $\tilde{\mathbf{G}}(\mathbf{L}, \mathbf{V} \tilde{\mathbf{x}})$  may not be a diagonal matrix).

In Fig. 4 we present the NMSPE versus the parameter  $\beta$ . It can be seen that the MSPE of the different estimators increases as  $\beta$  increases, since  $\beta$  is proportional to the variance of the unknown parameters. Moreover, the iterative estimators have significantly lower MSPE than the linear estimators for any  $\beta$ . In addition it can be seen that the eGFD-MAP and GSP-MAP estimator have similar MSPE values to those of the MAP estimator for any value of  $\beta$  that is large enough. Thus, in this case the proposed methods perform well even when the conditions of Theorem 2 are not satisfied.

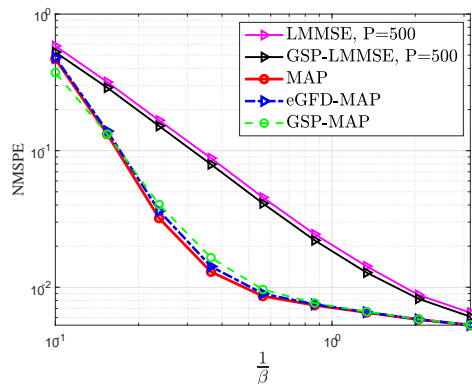


Fig. 4: The NMSPE of the different estimators versus  $\frac{1}{\beta}$  for 118-bus test case, where  $\sigma_w^2 = 0.05$ .

### C. Sensitivity to initialization

The implementation of the MAP estimator by the Gauss-Newton method is known to be sensitive to the initialization of the algorithm [20]. In this subsection, we examine the robustness of the MAP, eGFD-MAP, and GSP-MAP estimators to perturbed initialization under the same setting of the PSSE problem from Subsection V-B.

1) *Scenario I - noisy initialization*: In the first scenario, we use perturbed initialization, in which the estimators are initialized with

$$\hat{\mathbf{x}}^{(0)} = \mathbf{V}(\tilde{\mathbf{x}}_0 + \tilde{\mathbf{p}}_0), \quad (46)$$

where  $\tilde{\mathbf{x}}_0$  is the original initialization (i.e. the prior mean in the graph-frequency domain,  $\tilde{\boldsymbol{\mu}}_{\mathbf{x}}$ , or the GSP-LMMSE estimator in the graph frequency domain), and  $\tilde{\mathbf{p}}_0$  is zero-mean Gaussian noise with variance  $\sigma_p^2$ . The NMSPE of the estimators versus  $\frac{1}{\sigma_p^2}$  is presented in Fig. 5 for the 118-bus test case with this perturbed initialization.

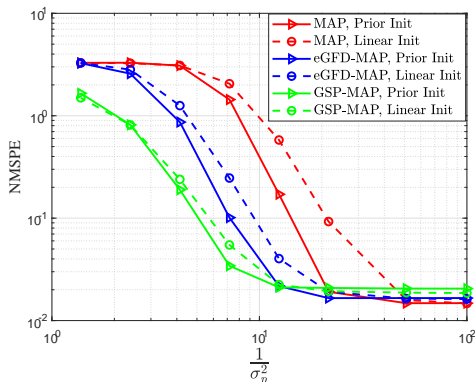


Fig. 5: The NMSPE of the different estimators versus  $\frac{1}{\sigma_p^2}$ , where the noisy GSP-LMMSE and the noisy prior mean were used to initialize each of the estimators, where  $\sigma_w^2 = 0.05$  and  $\beta = 3$ .

2) *Scenario II - Perturbed topology*: In the second scenario, the GSP-LMMSE and the LMMSE estimators were calculated under a change in the topology. In particular, the sample-mean versions of these estimators were calculated under a misspecified model. While the true dataset was generated with a given topology, the linear estimators assume a different topology obtained from the original topology after removing  $M$  edges. Then, the misspecified sample-mean GSP-LMMSE estimator was used as the initial estimator for the iterative estimators (similar results were obtained by using the misspecified sample-mean LMMSE estimator). Thus, this scenario describes a perturbed initialization, where the topology is perturbed and affects the initialization. The results are presented in Fig. 6 versus the number of removed edges  $M$ .

It can be seen in Figs. 5 and 6, associated with Scenarios I and II, respectively, that the MAP estimator is more sensitive to initialization than the proposed estimators. Specifically, when the noise variance is small or the number of removed edges is low, the MSPE of the MAP estimator is significantly larger than the MSPE of the proposed eGFD-MAP and GSP-MAP estimators. When comparing the initialization method, it can be seen that the eGFD-MAP and GSP-MAP estimators are more robust to the wrong initialization for both initialization methods (GSP-LMMSE and prior mean). Thus, we can conclude that when the initialization tends to be a problem, the proposed methods that use GSP information are preferable.

## VI. CONCLUSION

In this paper, we discuss the recovery of random graph signals from nonlinear measurements using a GSP-based MAP

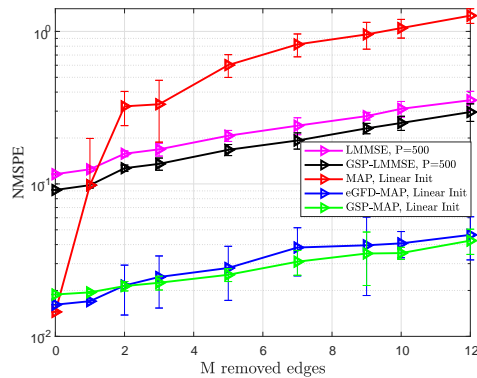


Fig. 6: The NMSPE of the different estimators versus the number of removed edges  $M$ , where the linear estimators (that were used to initialize the iterative estimators) were perturbed due to changes in the graph topology, where  $M$  edges were removed, where  $\sigma_w^2 = 0.05$  and  $\beta = 3$ .

approach. We formulate the MAP estimator in both the vertex and the graph-frequency domains, and show that although they lead to the same estimator, the efficiency and convergence rate of each implementation may be different. In order to accommodate the complexity and sensitivity to initialization of the MAP estimator, we developed the eGFD-MAP estimator that does not require a matrix inversion per iteration and can update the different elements of the graph signal in the graph-frequency domain independently. In addition, we derived the GSP-MAP estimator that is computed iteratively with an update equation that is composed of the output of two graph filters that are optimal in the sense of the expected objective function. We showed that when the measurement function is separable in the graph-frequency domain and the input graph signal and the noise vector are uncorrelated, the proposed eGFD-MAP and GSP-MAP estimators coincide with the conventional MAP estimator. We showed that the eGFD-MAP estimator has the lowest computational complexity, making its calculation tractable in large networks. Our numerical simulations show that the proposed eGFD-MAP and the GSP-MAP estimators achieve similar MSEs, compared to the MAP estimator, while the eGFD-MAP estimator is more efficient. Finally, We examined the sensitivity to initialization of the MAP estimator and showed that the eGFD-MAP and the GSP-MAP estimators are significantly more robust to perturbed and noisy initialization.

## APPENDIX A: INTERPRETATION OF THE MAP ESTIMATION PROBLEM AS A REGULARIZED WLS PROBLEM

For the special case where the distribution of the input graph signal,  $\mathbf{x}$ , in the graph-frequency domain is a smooth zero-mean Gaussian distribution [46], [47]:

$$\tilde{\mathbf{x}} \sim \mathcal{N}(\mathbf{0}, \beta \mathbf{\Lambda}^\dagger), \quad (47)$$

where  $\beta$  is the smoothness level. In this case,  $\boldsymbol{\mu}_{\mathbf{x}} = \mathbf{0}$  and  $\mathbf{C}_{\mathbf{x}\mathbf{x}} = \beta \mathbf{\Lambda}^\dagger$ , where  $(\cdot)^\dagger$  denotes the pseudo-inverse operator. By substituting this prior in (8), we obtain

$$Q(\mathbf{x}) = \frac{1}{2} \beta \mathbf{x}^T \mathbf{L} \mathbf{x} + \frac{1}{2} (\mathbf{y} - \mathbf{g}(\mathbf{L}, \mathbf{x}))^T \mathbf{C}_{\mathbf{w}\mathbf{w}}^{-1} (\mathbf{y} - \mathbf{g}(\mathbf{L}, \mathbf{x})). \quad (48)$$

The left term on the r.h.s. of (48),  $\frac{1}{2}\beta\mathbf{x}^T\mathbf{L}\mathbf{x}$ , can be interpreted as a regularization term, which corresponds to assuming that the graph signal  $\mathbf{x}$  is smooth on the graph.

If we take the model in (5) where the prior information can be neglected (e.g. when  $\mathbf{C}_{\mathbf{x}\mathbf{x}}$  is significantly larger than  $\mathbf{C}_{\mathbf{w}\mathbf{w}}$  in the positive-definite matrix sense), then we can develop the WLS estimator instead of the MAP estimator, as considered, for example, in [36]. In this case, we do not have the first term in the objective functions (e.g.  $\frac{1}{2}(\mathbf{x} - \boldsymbol{\mu}_{\mathbf{x}})^T \mathbf{C}_{\mathbf{x}\mathbf{x}}^{-1}(\mathbf{x} - \boldsymbol{\mu}_{\mathbf{x}})$  in (8)). However, we can add a Laplacian regularization term,  $\mu\mathbf{x}^T\mathbf{L}\mathbf{x}$ , to obtain the regularized WLS problem in (48). Signal recovery with a Laplacian regularization term has been used in various applications, such as image processing [50], [51] and state estimation in power systems [45].

#### APPENDIX B: PROOF OF THEOREM 1

For the sake of simplicity, in this appendix we use the notation  $\|\mathbf{a}\|_{\mathbf{B}} = \mathbf{a}^T\mathbf{B}\mathbf{a}$  for any vector  $\mathbf{a}$  and a positive semi-definite matrix  $\mathbf{B}$ . In addition, we use the short notations  $f_i(\mathbf{L})$ ,  $f_i(\boldsymbol{\Lambda})$ ,  $i = 1, 2$ , without writing explicitly the dependency on  $\hat{\mathbf{x}}^{(t)}$ . By substituting (22) in (12), we obtain

$$\begin{aligned} Q_{lin}(\hat{\mathbf{x}}^{(t+1)}, \hat{\mathbf{x}}^{(t)}) &= Q_{lin}(\hat{\mathbf{x}}^{(t)} + f_1(\mathbf{L})(\hat{\mathbf{x}}^{(t)} - \boldsymbol{\mu}_{\mathbf{x}}) \\ &\quad + f_2(\mathbf{L})(\mathbf{y} - \mathbf{g}(\mathbf{L}, \hat{\mathbf{x}}^{(t)})), \hat{\mathbf{x}}^{(t)}) \\ &= \frac{1}{2} \left\| (\mathbf{I} + f_1(\mathbf{L}))(\hat{\mathbf{x}}^{(t)} - \boldsymbol{\mu}_{\mathbf{x}}) \right. \\ &\quad \left. + f_2(\mathbf{L})(\mathbf{y} - \mathbf{g}(\mathbf{L}, \hat{\mathbf{x}}^{(t)})) \right\|_{\mathbf{C}_{\mathbf{x}\mathbf{x}}^{-1}} \\ &\quad + \frac{1}{2} \left\| -\mathbf{G}(\mathbf{L}, \hat{\mathbf{x}}^{(t)})f_1(\mathbf{L})(\hat{\mathbf{x}}^{(t)} - \boldsymbol{\mu}_{\mathbf{x}}) \right. \\ &\quad \left. + (\mathbf{I} - \mathbf{G}(\mathbf{L}, \hat{\mathbf{x}}^{(t)})f_2(\mathbf{L}))(\mathbf{y} - \mathbf{g}(\mathbf{L}, \hat{\mathbf{x}}^{(t)})) \right\|_{\mathbf{C}_{\mathbf{w}\mathbf{w}}^{-1}} \\ &= \frac{1}{2} \left\| (\mathbf{I} + f_1(\boldsymbol{\Lambda}))(\hat{\mathbf{x}}^{(t)} - \tilde{\boldsymbol{\mu}}_{\mathbf{x}}) \right. \\ &\quad \left. + f_2(\boldsymbol{\Lambda})(\tilde{\mathbf{y}} - \tilde{\mathbf{g}}(\mathbf{L}, \mathbf{V}\hat{\mathbf{x}}^{(t)})) \right\|_{\mathbf{C}_{\tilde{\mathbf{x}\mathbf{x}}}^{-1}} \\ &\quad + \frac{1}{2} \left\| -\tilde{\mathbf{G}}(\mathbf{L}, \mathbf{V}\hat{\mathbf{x}}^{(t)})f_1(\boldsymbol{\Lambda})(\hat{\mathbf{x}}^{(t)} - \tilde{\boldsymbol{\mu}}_{\mathbf{x}}) \right. \\ &\quad \left. + (\mathbf{I} - \tilde{\mathbf{G}}(\mathbf{L}, \mathbf{V}\hat{\mathbf{x}}^{(t)})f_2(\boldsymbol{\Lambda}))(\tilde{\mathbf{y}} - \tilde{\mathbf{g}}(\mathbf{L}, \mathbf{V}\hat{\mathbf{x}}^{(t)})) \right\|_{\mathbf{C}_{\tilde{\mathbf{w}\mathbf{w}}}^{-1}}, \quad (49) \end{aligned}$$

where the last equality is in the graph-frequency domain, which holds since  $\mathbf{V}$  is a unitary matrix, i.e.  $\mathbf{V}\mathbf{V}^T = \mathbf{I}$ .

Based on the assumption that  $\hat{\mathbf{x}}^{(t)}$  is close enough to  $\mathbf{x}$ , we replace  $\tilde{\mathbf{g}}(\mathbf{L}, \mathbf{V}\hat{\mathbf{x}}^{(t)})$  by  $\tilde{\mathbf{g}}(\mathbf{L}, \mathbf{V}\tilde{\mathbf{x}})$ , and  $\hat{\mathbf{x}}^{(t)} - \tilde{\boldsymbol{\mu}}_{\mathbf{x}}$  by  $\tilde{\mathbf{x}} - \tilde{\boldsymbol{\mu}}_{\mathbf{x}}$  in (49), but keep  $\tilde{\mathbf{G}}(\mathbf{L}, \mathbf{V}\hat{\mathbf{x}}^{(t)})$  evaluated at  $\hat{\mathbf{x}}^{(t)}$  (similar to the rationale behind the first-order approximation in the Gauss-Newton method [40]), to obtain the approximation

$$\begin{aligned} Q_{lin}^{approx}(\tilde{\mathbf{x}}, \hat{\mathbf{x}}^{(t)}) &= \\ &\frac{1}{2} \left\| (\mathbf{I} + f_1(\boldsymbol{\Lambda})(\tilde{\mathbf{x}} - \tilde{\boldsymbol{\mu}}_{\mathbf{x}}) + f_2(\boldsymbol{\Lambda})(\tilde{\mathbf{y}} - \tilde{\mathbf{g}}(\mathbf{L}, \mathbf{V}\tilde{\mathbf{x}})) \right\|_{\mathbf{C}_{\tilde{\mathbf{x}\mathbf{x}}}^{-1}} \\ &+ \frac{1}{2} \left\| -\tilde{\mathbf{G}}(\mathbf{L}, \mathbf{V}\hat{\mathbf{x}}^{(t)})f_1(\boldsymbol{\Lambda})(\tilde{\mathbf{x}} - \tilde{\boldsymbol{\mu}}_{\mathbf{x}}) \right. \\ &\quad \left. + (\mathbf{I} - \tilde{\mathbf{G}}(\mathbf{L}, \mathbf{V}\hat{\mathbf{x}}^{(t)})f_2(\boldsymbol{\Lambda}))(\tilde{\mathbf{y}} - \tilde{\mathbf{g}}(\mathbf{L}, \mathbf{V}\tilde{\mathbf{x}})) \right\|_{\mathbf{C}_{\tilde{\mathbf{w}\mathbf{w}}}^{-1}}. \quad (50) \end{aligned}$$

Our goal is to choose the filters  $f_1(\cdot)$  and  $f_2(\cdot)$  such that the objective  $Q_{lin}^{approx}$  is minimized on average. Thus, we minimize the expected cost from (50), under the assumption

that  $\tilde{\mathbf{x}}$  and  $\tilde{\mathbf{w}}$  are independent, and treating  $\tilde{\mathbf{G}}(\mathbf{L}, \mathbf{V}\hat{\mathbf{x}}^{(t)})$  as a deterministic matrix:

$$\begin{aligned} &\{f_1^*(\boldsymbol{\Lambda}), f_2^*(\boldsymbol{\Lambda})\} \\ &= \arg \min_{f_1(\boldsymbol{\Lambda}) \in \mathcal{D}_N, f_2(\boldsymbol{\Lambda}) \in \mathcal{D}_N} E[Q_{lin}^{approx}(\tilde{\mathbf{x}}, \hat{\mathbf{x}}^{(t)})], \quad (51) \end{aligned}$$

where  $E[Q_{lin}^{approx}(\tilde{\mathbf{x}}, \hat{\mathbf{x}}^{(t)})]$  is defined in (29). Since the minimization is separable w.r.t.  $f_1$  and  $f_2$ , we can solve it independently. Thus,

$$\begin{aligned} f_1^*(\boldsymbol{\Lambda}) &= \arg \min_{f_1(\boldsymbol{\Lambda}) \in \mathcal{D}_N} \sum_{n=1}^N [f_1(\boldsymbol{\Lambda})]_{n,n} \\ &+ \frac{1}{2} \sum_{n=1}^N \sum_{k=1}^N [\mathbf{C}_{\tilde{\mathbf{x}\mathbf{x}}}]_{n,k} [\mathbf{C}_{\tilde{\mathbf{x}\mathbf{x}}}^{-1}]_{k,n} [f_1(\boldsymbol{\Lambda})]_{k,k} [f_1(\boldsymbol{\Lambda})]_{n,n} \\ &+ \frac{1}{2} \sum_{n=1}^N \sum_{k=1}^N [\mathbf{C}_{\tilde{\mathbf{x}\mathbf{x}}}]_{n,k} [\mathbf{A}]_{k,n} [f_1(\boldsymbol{\Lambda})]_{k,k} [f_1(\boldsymbol{\Lambda})]_{n,n}. \quad (52) \end{aligned}$$

By equating the derivative of (52) w.r.t.  $[f_1(\boldsymbol{\Lambda})]_{l,l}$  to zero, one obtains

$$\begin{aligned} 0 &= 1 + \sum_{n=1}^N [\mathbf{C}_{\tilde{\mathbf{x}\mathbf{x}}}]_{n,l} [\mathbf{C}_{\tilde{\mathbf{x}\mathbf{x}}}^{-1}]_{l,n} [f_1^*(\boldsymbol{\Lambda})]_{n,n} \\ &+ \sum_{n=1}^N [\mathbf{C}_{\tilde{\mathbf{x}\mathbf{x}}}]_{n,l} [\mathbf{A}]_{l,n} [f_1^*(\boldsymbol{\Lambda})]_{n,n}, \quad \forall l = 1, \dots, N, \quad (53) \end{aligned}$$

which results in

$$\text{diag}(f_1^*(\boldsymbol{\Lambda})) = -(\mathbf{C}_{\tilde{\mathbf{x}\mathbf{x}}} \circ \mathbf{C}_{\tilde{\mathbf{x}\mathbf{x}}}^{-1} + \mathbf{C}_{\tilde{\mathbf{x}\mathbf{x}}} \circ \mathbf{A})^{-1} \mathbf{1}. \quad (54)$$

By applying the diag operator on both sides of (54) and substituting (30), we obtain the graph filter in (27).

Similarly, the optimization w.r.t. the filter  $f_2(\boldsymbol{\Lambda})$  is

$$\begin{aligned} f_2^*(\boldsymbol{\Lambda}) &= \arg \min_{f_2(\boldsymbol{\Lambda}) \in \mathcal{D}_N} \\ &\frac{1}{2} \sum_{n=1}^N \sum_{k=1}^N [\mathbf{C}_{\tilde{\mathbf{w}\mathbf{w}}}]_{n,k} [\mathbf{C}_{\tilde{\mathbf{x}\mathbf{x}}}^{-1}]_{k,n} [f_2(\boldsymbol{\Lambda})]_{k,k} [f_2(\boldsymbol{\Lambda})]_{n,n} \\ &\quad - \sum_{n=1}^N [\tilde{\mathbf{G}}(\mathbf{L}, \mathbf{V}\hat{\mathbf{x}}^{(t)})]_{n,n} [f_2(\boldsymbol{\Lambda})]_{n,n} \\ &+ \frac{1}{2} \sum_{n=1}^N \sum_{k=1}^N [\mathbf{C}_{\tilde{\mathbf{w}\mathbf{w}}}]_{n,k} [\mathbf{A}]_{k,n} [f_2(\boldsymbol{\Lambda})]_{k,k} [f_2(\boldsymbol{\Lambda})]_{n,n}. \quad (55) \end{aligned}$$

By equating the derivative of (55) w.r.t.  $[f_2(\boldsymbol{\Lambda})]_{l,l}$  to zero, one obtains

$$\begin{aligned} 0 &= \sum_{n=1}^N [\mathbf{C}_{\tilde{\mathbf{w}\mathbf{w}}}]_{n,l} [\mathbf{C}_{\tilde{\mathbf{x}\mathbf{x}}}^{-1}]_{l,n} [f_2^*(\boldsymbol{\Lambda})]_m \\ &\quad - [\tilde{\mathbf{G}}(\mathbf{L}, \mathbf{V}\hat{\mathbf{x}}^{(t)})]_{l,l} + \sum_{n=1}^N [\mathbf{C}_{\tilde{\mathbf{w}\mathbf{w}}}]_{n,l} [\mathbf{A}]_{l,n} [f_2^*(\boldsymbol{\Lambda})]_m, \quad (56) \end{aligned}$$

$\forall l = 1, \dots, N$ , which results in

$$\begin{aligned} &\text{diag}(f_2^*(\boldsymbol{\Lambda})) \\ &= (\mathbf{C}_{\tilde{\mathbf{w}\mathbf{w}}} \circ \mathbf{C}_{\tilde{\mathbf{x}\mathbf{x}}}^{-1} + \mathbf{C}_{\tilde{\mathbf{w}\mathbf{w}}} \circ \mathbf{A})^{-1} \text{diag}(\tilde{\mathbf{G}}(\mathbf{L}, \mathbf{V}\hat{\mathbf{x}}^{(t)})). \quad (57) \end{aligned}$$

By applying the diag operator on both sides of (57) and substituting (30), we obtain the graph filter in (28).

## REFERENCES

- [1] A. Ortega, P. Frossard, J. Kovačević, J. M. F. Moura, and P. Vandergheynst, "Graph signal processing: Overview, challenges, and applications," *Proc. IEEE*, vol. 106, no. 5, pp. 808–828, May 2018.
- [2] D. I. Shuman, S. K. Narang, P. Frossard, A. Ortega, and P. Vandergheynst, "The emerging field of signal processing on graphs: Extending high-dimensional data analysis to networks and other irregular domains," *IEEE Signal Processing Magazine*, vol. 30, no. 3, pp. 83–98, May 2013.
- [3] E. Isufi, A. Loukas, A. Simonetto, and G. Leus, "Autoregressive moving average graph filtering," *IEEE Trans. Signal Process.*, vol. 65, no. 2, pp. 274–288, 2017.
- [4] D. I. Shuman, B. Ricaud, and P. Vandergheynst, "A windowed graph fourier transform," in *2012 IEEE Statistical Signal Processing Workshop (SSP)*, Aug. 2012, pp. 133–136.
- [5] Y. Tanaka, Y. C. Eldar, A. Ortega, and G. Cheung, "Sampling signals on graphs: From theory to applications," *IEEE Signal Processing Magazine*, vol. 37, no. 6, pp. 14–30, 2020.
- [6] A. Anis, A. Gadde, and A. Ortega, "Towards a sampling theorem for signals on arbitrary graphs," in *Proc. of ICASSP*, May 2014, pp. 3864–3868.
- [7] A. G. Marques, S. Segarra, G. Leus, and A. Ribeiro, "Sampling of graph signals with successive local aggregations," *IEEE Trans. Signal Process.*, vol. 64, no. 7, pp. 1832–1843, Apr. 2016.
- [8] Z. Xiao, H. Fang, and X. Wang, "Distributed nonlinear polynomial graph filter and its output graph spectrum: Filter analysis and design," *IEEE Trans. Signal Processing*, vol. 69, pp. 1–15, 2021.
- [9] G. B. Giannakis, Y. Shen, and G. V. Karanikolas, "Topology identification and learning over graphs: Accounting for nonlinearities and dynamics," *Proc. IEEE*, vol. 106, no. 5, pp. 787–807, 2018.
- [10] Y. Shen, G. B. Giannakis, and B. Baingana, "Nonlinear structural vector autoregressive models with application to directed brain networks," *IEEE Trans. Signal Process.*, vol. 67, no. 20, pp. 5325–5339, 2019.
- [11] Z. Xiao and X. Wang, "Nonlinear polynomial graph filter for signal processing with irregular structures," *IEEE Trans. Signal Processing*, vol. 66, no. 23, pp. 6241–6251, 2018.
- [12] E. Drayer and T. Rauttenberg, "Detection of false data injection attacks in smart grids based on graph signal processing," *IEEE Systems Journal*, vol. 14, no. 2, pp. 1886–1896, 2020.
- [13] S. Grotas, Y. Yakoby, I. Gera, and T. Rauttenberg, "Power systems topology and state estimation by graph blind source separation," *IEEE Trans. Signal Processing*, vol. 67, no. 8, pp. 2036–2051, 2019.
- [14] S. Shaked and T. Rauttenberg, "Identification of edge disconnections in networks based on graph filter outputs," *IEEE Trans. Signal and Information Processing over Networks*, 2021.
- [15] O. Edfors, M. Sandell, J. J. van de Beek, S. K. Wilson, and P. O. Borjesson, "OFDM channel estimation by singular value decomposition," in *Proc. of Vehicular Technology Conference*, vol. 2, 1996, pp. 923–927.
- [16] N. Geng, X. Yuan, and L. Ping, "Dual-diagonal LMMSE channel estimation for OFDM systems," *IEEE Trans. Signal Process.*, vol. 60, no. 9, pp. 4734–4746, 2012.
- [17] I. E. Berman and T. Rauttenberg, "Partially linear bayesian estimation using mixed-resolution data," *IEEE Signal Processing Letters*, vol. 28, pp. 2202–2206, 2021.
- [18] A. Kroizer, T. Rauttenberg, and Y. C. Eldar, "Bayesian estimation of graph signals," *IEEE Trans. Signal Processing*, vol. 70, pp. 2207–2223, 2022.
- [19] A. Amar and T. Rauttenberg, "Widely-linear mmse estimation of complex-valued graph signals," *Arxiv, submitted to IEEE Trans. Signal Processing*, 2022. [Online]. Available: <https://arxiv.org/abs/2208.10588>
- [20] M. Fatemi, L. Svensson, L. Hammarstrand, and M. Morelande, "A study of MAP estimation techniques for nonlinear filtering," in *2012 15th International Conference on Information Fusion*, 2012, pp. 1058–1065.
- [21] B. Blaschke, A. Neubauer, and O. Scherzer, "On convergence rates for the iteratively regularized Gauss-Newton method," *IMA Journal of Numerical Analysis*, vol. 17, pp. 421–436, 1997.
- [22] —, "On convergence rates for the iteratively regularized Gauss-Newton method," *IMA Journal of Numerical Analysis*, vol. 17, no. 3, pp. 421–436, June 1997.
- [23] S. Chen, A. Sandryhaila, J. M. F. Moura, and J. Kovacevic, "Signal denoising on graphs via graph filtering," in *Proc. of GlobalSIP*, 2014, pp. 872–876.
- [24] F. Zhang and E. R. Hancock, "Graph spectral image smoothing using the heat kernel," *Pattern Recognition*, vol. 41, pp. 3328 – 3342, 2008.
- [25] S. Chen, F. Cerda, P. Rizzo, J. Bielak, J. H. Garrett, and J. Kovačević, "Semi-supervised multiresolution classification using adaptive graph filtering with application to indirect bridge structural health monitoring," *IEEE Trans. Signal Process.*, vol. 62, no. 11, pp. 2879–2893, 2014.
- [26] S. Chen, A. Sandryhaila, J. M. F. Moura, and J. Kovačević, "Signal recovery on graphs: Variation minimization," *IEEE Trans. Signal Process.*, vol. 63, no. 17, pp. 4609–4624, Sept. 2015.
- [27] N. Perraudin and P. Vandergheynst, "Stationary signal processing on graphs," *IEEE Trans. Signal Process.*, vol. 65, pp. 3462–3477, 2017.
- [28] L. Ruiz, F. Gama, and A. Ribeiro, "Graph neural networks: Architectures, stability, and transferability," *Proceedings of the IEEE*, vol. 109, no. 5, pp. 660–682, 2021.
- [29] F. Gama, E. Isufi, G. Leus, and A. Ribeiro, "Graphs, convolutions, and neural networks: From graph filters to graph neural networks," *IEEE Signal Processing Magazine*, vol. 37, no. 6, pp. 128–138, 2020.
- [30] Q. Yang, A. Sadeghi, G. Wang, G. B. Giannakis, and J. Sun, "Power system state estimation using Gauss-Newton unrolled neural networks with trainable priors," in *2020 IEEE International Conference on Communications, Control, and Computing Technologies for Smart Grids (SmartGridComm)*, 2020, pp. 1–6.
- [31] J. Mei and J. M. F. Moura, "Signal processing on graphs: Causal modeling of unstructured data," *IEEE Trans. Signal Processing*, vol. 65, no. 8, pp. 2077–2092, 2017.
- [32] F. Hua, R. Nassif, C. Richard, H. Wang, and A. H. Sayed, "Online distributed learning over graphs with multitask graph-filter models," *IEEE Trans. Signal Inf. Process. Netw.*, vol. 6, pp. 63–77, 2020.
- [33] A. Kroizer, Y. C. Eldar, and T. Rauttenberg, "Modeling and recovery of graph signals and difference-based signals," in *Proc. of GlobalSIP*, Nov. 2019, pp. 1–5.
- [34] N. Shlezinger and T. Rauttenberg, "Discriminative and generative learning for linear estimation of random signals (lecture notes)," *Arxiv*, 2022. [Online]. Available: <http://arxiv.org/abs/2206.04432>
- [35] A. K. Sahu, D. Jakovetic, D. Bajovic, and S. Kar, "Communication efficient distributed weighted non-linear least squares estimation," *EURASIP Journal on Advances in Signal Processing*, vol. 2018, no. 1, pp. 1–15, 2018.
- [36] A. K. Sahu, S. Kar, J. M. F. Moura, and H. V. Poor, "Distributed constrained recursive nonlinear least-squares estimation: Algorithms and asymptotics," *IEEE Trans. Signal and Information Processing over Networks*, vol. 2, no. 4, pp. 426–441, 2016.
- [37] D. P. Bertsekas, Ed., *Nonlinear Programming*, 2nd ed. MA, USA: Athena Scientific, 1999.
- [38] B. Bell and F. Cathey, "The iterated Kalman filter update as a Gauss-Newton method," *IEEE Trans. Automatic Control*, vol. 38, no. 2, pp. 294–297, 1993.
- [39] P. Deuffhard and G. Heindl, "Affine invariant convergence theorems for Newton's method and extensions to related methods," *SIAM Journal on Numerical Analysis*, vol. 16, no. 1, pp. 1–10, 1979.
- [40] B. Bell and F. Cathey, "The iterated Kalman filter update as a Gauss-Newton method," *IEEE Trans. Automatic Control*, vol. 38, no. 2, pp. 294–297, 1993.
- [41] G. Golub and V. Pereyra, "Separable nonlinear least squares: the variable projection method and its applications," *Inverse problems*, vol. 19, no. 2, p. R1, 2003.
- [42] W. D. J., Strogatz, and S. H., "Collective dynamics of small-world networks," *Nature*, pp. 393–440, 1998.
- [43] A. Abur and A. Gomez-Exposito, *Power System State Estimation: Theory and Implementation*. Marcel Dekker, 2004.
- [44] D. Bienstock and A. Verma, "Strong NP-hardness of AC power flows feasibility," *Oper. Res. Lett.*, vol. 47, no. 6, pp. 494–501, 2019.
- [45] L. Dabush, A. Kroizer, and T. Rauttenberg, "State estimation in unobservable power systems via graph signal processing tools," 2021. [Online]. Available: <https://arxiv.org/abs/2106.02254>
- [46] X. Dong, D. Thanou, P. Frossard, and P. Vandergheynst, "Learning Laplacian matrix in smooth graph signal representations," *IEEE Trans. Signal Process.*, vol. 64, no. 23, pp. 6160–6173, Dec. 2016.
- [47] M. Ramezani-Mayiami, M. Hajimirsadeghi, K. Skretting, R. S. Blum, and H. V. Poor, "Graph topology learning and signal recovery via Bayesian inference," in *DSW*, 2019, pp. 52–56.
- [48] "Power systems test case archive." [Online]. Available: <http://www.ee.washington.edu/research/pstca/>
- [49] T. Rauttenberg and J. Tabrikian, "Bayesian parameter estimation using periodic cost functions," *IEEE Trans. Signal Processing*, vol. 60, no. 3, pp. 1229–1240, 2012.
- [50] M. Zheng, J. Bu, C. Chen, C. Wang, L. Zhang, G. Qiu, and D. Cai, "Graph regularized sparse coding for image representation," *IEEE Trans. Image Processing*, vol. 20, no. 5, pp. 1327–1336, May 2011.
- [51] A. Elmoataz, O. Lezoray, and S. Boughleux, "Nonlocal discrete regularization on weighted graphs: A framework for image and manifold processing," *IEEE Trans. Image Processing*, vol. 17, no. 7, pp. 1047–1060, July 2008.